FABRICATION AND ANALYSIS OF PLASTIC HYPODERMIC NEEDLES BY MICRO INJECTION MOLDING

A Thesis
Presented to
The Academic Faculty

By

Hoyeon Kim

In Partial Fulfillment of
the Requirements for
the Degree Master of Science
in Mechanical Engineering

Georgia Institute of Technology

May 2004

FABRICATION AND ANALYSIS OF PLASTIC HYPODERMIC NEEDLES BY MICRO INJECTION MOLDING

Approved by:

Dr. Jonathan S. Colton, ME, Chair

Dr. John D. Muzzy, CHE

Dr. Suresh K. Sitaraman, ME

Dr. Robert Chen, CDC

April 9, 2004

"It is almost a definition of a gentleman to say that he is one who never inflicts pain."

in The Idea of a University (1873) Discourse VIII

John Henry Cardinal Newman (1801-1890)

ACKNOWLEDGMENTS

First of all, I would like to thank my advisor, Dr. Jonathan S. Colton for always expecting my best. He gave me this opportunity and support to perform research. He gave me invaluable guidance and advice when I felt things were going wrong. His expectations and faith in my capabilities were driving forces to break through difficulties during this research.

I also thank Drs. Suresh Sitaraman, John Muzzy and Robert Chen for serving on my thesis reading committee, as well as for serving as references for the research. They gave me good advice to find the right way at moments of choice. In addition to this, I thank the Georgia Tech-CDC seed grant program for funding this research. I also thank Dr. Bruce Weniger of the CDC for his invaluable advice.

This research would not have been possible without the technical support of the Georgia Institute of Technology. I appreciate the assistance of the staff in the ME machine shop, especially Steven Sheffield. They trained me to use all the machines in the shop and to translate my drawings into the real world parts. Without their help, I would not have been able to bring all my thinking and drawing to reality and complete this research. I thank Dr. Jung-Hwan Park and the people in IBB for letting me use the testing machine there.

I am thankful to the members of Center for Polymer Processing at Georgia Tech for their support and friendship. I thank Andy McFarland, Erick Rios, Heather Heffner, and Andy Song for helpful discussions and insight during this research. I thank Dr. Young-bin Park for giving me various advice and support not only for research but also for living

in Atlanta. And I also thank students from Chemical Engineering department, Bryan Shaw, Yanyan Tang, Pretish Patel, Susnata Samanta and Latoya Bryson for giving me help and advice for finishing this research.

I would like to thank my parents and sisters for their priceless support, guidance, and love. First of all, my father, Ju-Won Kim introduced me to engineering and gave me advice and strength when I had to make the important choice to be here. I give a special appreciation to my mother, Young-Ja Hong for always praying for me. I thank Aunt Young-Hee Hong for praying for me and giving me positive cheer all the time and congratulate her on her marriage in March. I also thank my sister Jeong-Yeon Kim Lee and her children, Linus and Annette, for cheering me up from Knoxville, TN and Shin-Yeon Kim and Jae-Yeon Kim for warm words of encouragement from Korea. Finally and most of all, I give tremendous thanks to God for leading me to do this research and finish this thesis.

TABLE OF CONTENTS

LIST OF TABLES

LIST OF FIGURES

LIST OF SYMBOLS

A	Cross sectional area
E	Young's modulus
I	Second moment of inertia
k	Buckling coefficient determined by the boundary condition of loading
L	Length of needle
L_{cr}	Critical length at which material yields in compression before buckling
P_{cr}	Buckling critical load
SC	Stratum corneum layer; most outer layer of skin
S_Y	Compressive yield stress of material
μ	Coefficient of friction

SUMMARY

This thesis explores the analysis and fabrication of plastic hypodermic needles. The hypotheses for this work are that replacing metal hypodermic needles with plastic ones will reduce or eliminate the possibility of the second-hand infections from needle sticks and unsterlized reuse and will be more cost and time efficient to recycle.

The most critical structural failure mode for plastic needles is buckling due to their shape (thin walled hollow column). The consideration of buckling is critical to avoid structural failure and to ensure reliability for medical applications. The buckling strength of a cannula is analyzed by analytic (Euler buckling theory) and finite element analysis (FEA) methods. A 22 gage needle model (OD 0.7mm, ID 0.4mm, Length 12.7mm) was analyzed. Euler buckling theory was used to calculate the critical buckling load. Numerical approaches using finite element analyses showed very similar results with analytic results. A skin model was introduced to simulate boundary conditions in the numerical approaches.

To verify the results of the analyses, cannulas with the same cross-sectional dimensions were fabricated using a micro injection molding technique. To make the parts hollow, a core assembly of straightened wire was used. Using the tip of a 22 gage needle, cannulas with the inverse shape of an actual hypodermic needle were made.

The structural (buckling) characteristics of cannulas were measured by a force-displacement testing machine. When buckling occurred, an arch shape was visible and there was an abrupt change in the load plot. Test results showed the relation between the needle's length and the buckling load, which was similar to that predicted by Euler

buckling theory. However, test values were 60% of the theoretical or analytical results. Several reasons to explain these discrepancies can be found. The first is that an unexpected bending moment resulted from an eccentric loading due to installation off-center to the center of the testing machine or to the oblique insertion. A cannula that was initially bent during ejection from the mold can add an unexpected bending moment. The quality control of cannulas can be another reason. Bent or misaligned core wires produce eccentric cannulas, and the thinner wall section can buckle or initiate fracture more easily. The last reason may be that Euler buckling theory is not fully valid in short cannula, because the axial stress reaches yield stress before buckling occurs. Inelastic deformation occurs (i.e., the modulus is reduced) during compression in short cannula. The Johnson column formula is introduced to explain this situation. Especially for the nylon nanocomposite material tested, a loss in modulus due to moisture absorption may be another explanation for the discrepancies.

CHAPTER 1

INTRODUCTION

This thesis investigated the fabrication and physical characteristics of plastic hypodermic needles. Some efforts have been made to replace metal hypodermic needles with plastic ones. However, plastics are intrinsically weaker than metals. Therefore, structural consideration is very critical to avoid failure and ensure reliability for medical applications. In this research, the fabrication of a cannula structure and its structural analysis will be studied. Theoretical analyses will be verified by the measurement of the buckling stresses. By fabricating and testing cannulas, the feasibility of replacing metallic hypodermic needles by plastic ones will be explored.

1.1 INTRODUCTION TO PLASTIC HYPODERMIC NEEDLES

For many decades, medical workers have used metal hypodermic needles to inject medicine into or to obtain blood from patients. These needles have many weak points, such as infection from multiple, unsterlized uses, and needle stick problems. As hypodermic needle technology improved, injections have become safer, less painful, and more common. However, in the developing world, these problems have not been reduced much. It is thought that more than half of injections in the developing world are unsafe, exposing patients to the risk of infection with hepatitis, HIV and other blood-borne

pathogens **[1]**. Many second-hand infections resulting from multiple usages of needles without proper sterilization have been reported.

Many ideas have been proposed to prevent multiple uses. Devices to restrict the movement of plungers in syringes and check valves to restrict the direction of flow are examples.

1.1.1 Advantages of Plastic for Hypodermic Needles

A hypodermic needle made of plastic will be easily disposed. Plastic materials can be degraded or melted at relatively low temperatures. In comparison, metals need to be heated to temperatures higher than 1000 ℃ to melt. In the developing world, high temperature incineration facilities are rare and not cost effective. This is one reason why metal needles are used multiple times.

Plastic needles can be disposed of or disabled very easily. Due to its lower melting point and strength, there is no need to heat up or to smash a needle to destroy it. After usage, it can be put into ordinary recycling process without special treatment, such as separation of metal needles from plastic syringes.

In addition, plastics are more flexible and softer than metals, which is advantageous for intravenous (IV) catheters (Fig 1.1) to reduce a patient's pain during IV injections. However these catheters cannot penetrate skin by themselves, they are installed with help of a metal needle. A plastic needle that is more flexible and softer than steel and is stiffer than a catheter will be able to penetrate skin. It may also reduce pain during injection, because a flexible needle will do less harm on tissues and give less pain to patients.

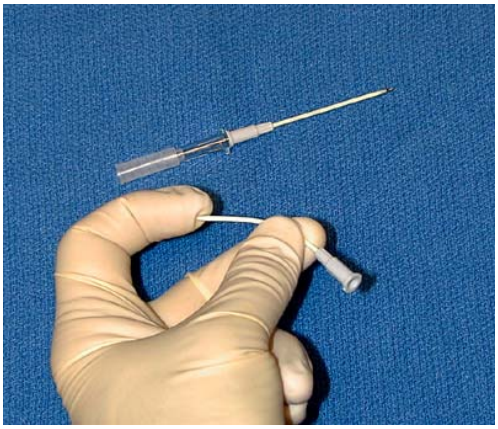

Fig 1.1: Intravenous (IV) Catheter

1.1.2 Disadvantages of Plastic Hypodermic Needles

The biggest disadvantage of plastic hypodermic needles is their strength. Plastic is weak compared to the steels used for metal needles. The modulus of plastic is typically 1% of that of steel. The mechanical properties of several plastics and steel are shown in Table 1.1.

Because of this weak point, a needle may break and remain in the body after injection. These disadvantages have hindered the acceptance of plastic hypodermic needles. However stronger and tougher materials are now available, due to improvements in material science. In this research, a nylon 6 nanocomposite material from Honeywell is used to make needles. This material is made of nylon 6 and nano-clay (MONTMORILLONITE). This material shows 20% and 58% increases in modulus in the machine direction and transverse direction, respectively, as compared to the neat resin **[4]**. Materials are discussed in detail in Chapter 3.

Table 1.1: Mechanical Properties of Commonly Used Materials [2]

	Nylon 66	PE	PMMA	PC	Steel
Density (g / cm^3)	1.14	0.94	1.18	1.2	6.92-9.13
Tensile strength (MPa)	76	28-36	55-76	63	205-1705
Elongation (%)	90	400-900	30 Max	60-100	36
Modulus (GPa)	2.8	0.71	2.96-3.28	2.45	190-210

1.2 INTRODUCTION TO MICROINJECTION MOLDING

Injection molding of plastic materials typically is performed in machines (Fig 1.2). Injection molding is optimized for mass production and for the production of large volume parts. A large amount of plastic is melted in the barrel. However, it takes only a few pellets of plastic to make a hypodermic needle or other micro-scale part. So there is a large amount of molten plastic in the barrel when making small parts on a large machine. During processing, this molten plastic can easily degrade due to long residence times. This reduces the mechanical properties of the final parts. Therefore, traditional machines are not appropriate for molding micro parts.

To overcome this problem in this research, a Sesame™ .080 Nanomolding™ (Medical Murray Inc. Buffalo Grove, IL 60089) machine is used, which is optimized for micro parts with small volumes. This machine does not have a screw to melt the plastic pellets, but rather a plunger and block to melt a small amount of plastic, which is enough

for several shots. Fig 1.3 is a picture of the Sesame™ .080 nanomolding™ machine, and Fig 1.4 shows its injection unit.

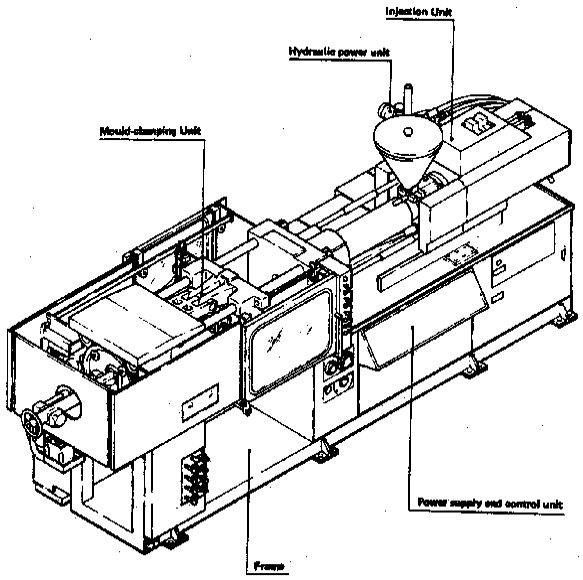

Fig 1.2: Injection molding machine [6]

Fig 1.3: Sesame™ .080 nanomolding™ machine.

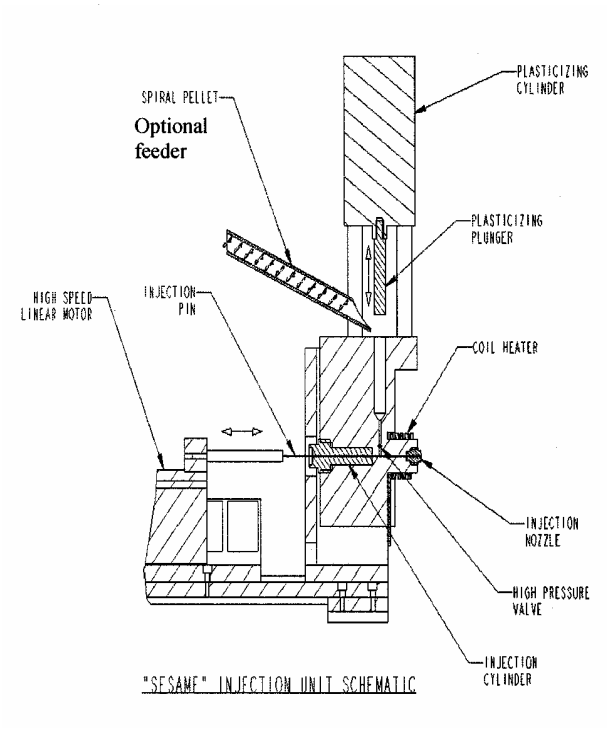

Fig 1.4: Schematic of Sesame™ .080 Nanomolding™ machine [7]

1.3 GOAL

This thesis presents the fabrication of a 22-gage (OD: 0.71mm, ID: 0.38mm) cannula body from plastic and characterizes its properties. The goal of this thesis is to determine the range of axial stresses that its cannula body can sustain. This range is a crucial factor that determines tip sharpness. The sharper the tip is, the smaller is the force needed to penetrate the skin. A smaller penetration force also means reduced axial force exerted on the cannula and less pain for the patient. Unfortunately, plastics cannot be sharpened by conventional grinding. Rather, plastic needles should be made using a mass

production technique such as injection molding. The range of axial stress that a cannula needle body can withstand will be important in designing the needle and hence the mold to make it. A sharp tip and the control of its quality are very crucial in making a successful plastic needle.

1.4 THESIS ORGANIZATION

Chapter 2 explores the structural properties of a cannula, and analytical and numerical analyses of buckling are presented. Buckling in classical mechanics is reviewed in order to approximate the critical load, and a more accurate finite element analysis is described. In addition, a simulation of skin penetration is described.

Chapter 3 presents the design and fabrication of plastic hypodermic needles, mold making, and injection molding of plastic hypodermic needles. Material candidates for consideration also will be listed. Consideration of many aspects (such as mechanical properties and biocompatibility) is performed. The design of the mold and the core alignment method are presented. Traditional mold fabrication techniques and non-conventional machining techniques used in mold making also are described.

Chapter 4 presents the experiments that measured the mechanical properties of the needles made in Chapter 3. In this chapter, the testing machine, experimental parameters, and experimental set-up will be shown. Also, the test results will be presented.

Chapter 5 presents a discussion of the experimental results presented in Chapter 4. A comparison with the theoretical results from Chapter 2 is presented. Trends of the

experimental results are considered, and explanations for the differences between theoretical and experimental results will be presented.

Chapter 6 presents the conclusions of this work and recommendations for future work.

CHAPTER 2

THEORY AND ANALYSIS

When a needle penetrates the skin, the maximum principal stress on the needle is axial. The configuration of the needle is a thin-walled column under axial load, which is very susceptible to buckling failure. Therefore, a buckling analysis is crucial in any structural analysis. In this chapter, a review of classical buckling mechanics will be presented. Also, using finite element methods, numerical analyses of buckling and skin penetration will be presented. The results of the buckling analyses will be compared to the experimental results in Chapter 6.

2.1 THEORY

Buckling occurs when the force equilibrium becomes unstable and is disturbed slightly from its equilibrium configuration. Every structure has a critical load that induces unstable equilibrium. The same structure can have different critical loads depending on support and load configurations. This will be discussed below.

2.1.1 BASIC ANALYTIC SOLUTION

The critical load which induces a vertical column system into unstable equilibrium (buckling) can be calculated analytically. The basic analytic approach to buckling of simple long columns is that of Euler [8]. The governing equation is Eq. (2.1)

$$EI\,v'' + P\,v = 0 \tag{2.1}$$

where E is the Young's modulus of the material, I is the second moment of inertia of the cross-section, v" is the second derivative of the lateral deflection, P is the axial load, and v is the lateral deflection. This is the simplest and the most non-conservative approach to buckling. If there is an eccentric load or inelastic condition (such as in intermediate-length cannula) involved, buckling occurs at a lower axial load or in a non-specific pattern. In this equation, the buckling occurs when this equation has trivial solutions (singularities). From analytic calculations, singularities happen when P is multiple of P_{CR} (the critical buckling load). From analytic calculations, P_{CR} is written as Eq. (2.2).

$$P_{CR} = k\frac{EI}{L^2} \tag{2.2}$$

where k is a constant determined by the support conditions (boundary conditions). Table 2.1 shows k values for various support configurations. L is length of the column. This solution is valid only when the length of the column is comparatively long.

For short-length-columns, this formula is not fully valid due to compressive yield of the materials. Of the several explanations proposed, the Johnson column formula is the most commonly used. It will be discussed later.

The configuration when the needle is penetrating the skin can be classified as any of the conditions shown in Fig 2.1, excluding the pinned-pinned condition. The needle is firmly fixed to the syringe. However there is only friction between the needle tip and the

skin. Depending on the friction between the skin and the needle tip, the supporting condition can be considered either rotating or fixed. Actual cases, such as eccentric loading and inelastic deformation condition in intermediate-length-column, will be discussed in Chapter 5.

Table 2.1: Constants k in critical buckling load for each configuration [9]

Pinned-pinned	Fixed-free	Fixed-fixed	Fixed-pinned
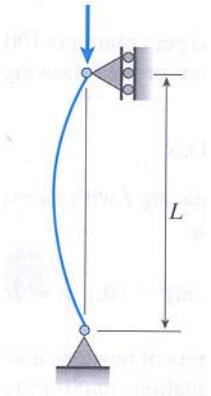	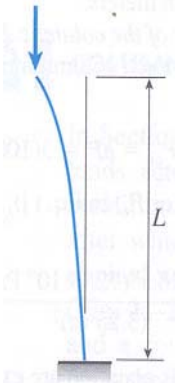	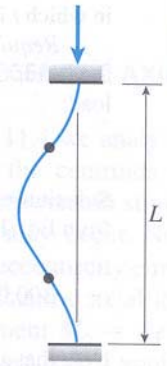	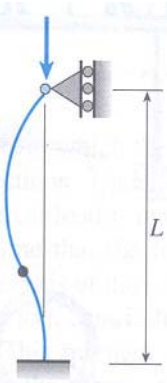
$k = \pi^2$	$k = \frac{\pi^2}{4}$	$k = 4\pi^2$	$k = 2.046\pi^2$

2.1.2 RESULT

To calculate the critical buckling load of a cannula, the dimensions of the needle are required. Table 2.2 shows the dimensions of a 22 gage needle and data made with a nano-composite nylon. The second moment of inertia (I) of the cannula is calculated by Eq 2.3

Table 2.2: Properties of a 22 gage needle

OD (mm)		0.712
ID (mm)		0.394
L (mm)		12.7
E (MPa)	(Dry)	4000
	(Measured)	2900

$$I = \frac{\pi}{64}\left(OD^4 - ID^4\right) \tag{2.3}$$

where OD is outer diameter of the cross-section and ID is inner diameter of the cross section. The length is determined by the dimensions of the mold and is used to compare to the results from actual testing. E is a material constant; XA-2908 nylon 6 nanocomposite (Honeywell) is used in this thesis. More data for XA-2908 nylon 6 nanocomposite material are shown in Appendix 1. From these data and Eq (2.2), I is calculated to be 0.011338(m). P_{CR} for each case is shown in Table 2.3. However, the moduli of nylon-matrix-materials are very sensitive to moisture. The measured modulus value is from tensile tests (ASTM 638D). Numerical analyses are performed with the "dry" values. But in the validation with the mechanical testing of the real parts, the values will be recalculated from the measured modulus.

Table 2.3: Buckling critical load

Supporting Condition	Fixed-free	Fixed-fixed	Fixed-pinned
Diagram	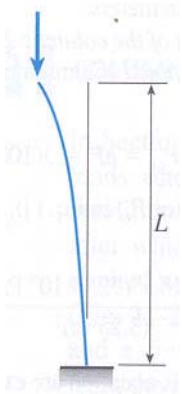	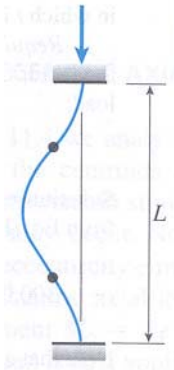	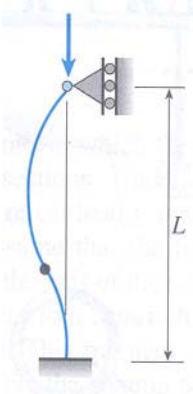
k	$k = \frac{\pi^2}{4}$	$k = 4\pi^2$	$k = 2.046\pi^2$
P_{CR} (N)	1.40	11.19	5.73

2.2 FINITE ELEMENT ANALYSIS (FEA)

As the effect of friction between skin and the tip of a needle is not known, it is not easy to tell which support condition is dominant. In this section, analyses using finite element techniques which include friction are presented. Ansys® release 7.0 (ANSYS, Inc., Canonsburg, PA) is the FEA used. In addition, a simulation of poking a cannula against skin is provided. In this analysis, the stress distribution and deformed shape of the skin model is considered to obtain criteria for penetration of skin.

2.2.1 SIMPLE COMPRESSION AND BUCKLING

To start, the compression of a simple concentric tube is analyzed without considering skin or other complex conditions. The result of this analysis is compared to the analytic result. Comparison of these is used to verify that the finite element method can find the critical buckling load.

2.2.1.1 MODELING AND MESHING

A simple concentric tube-shaped model is used. The dimensions are the same as above (Table 2.2). Fig 2.1 shows the meshing of the model with a mesh size 0.15mm. Meshing was performed using the Solid95 element type. To ensure the convergence of results, various mesh sizes (0.15mm, 0.12mm, 0.09mm) were used. By using linear regression, convergence values were obtained.

The Solid95 element type is defined by 20 nodes having three degrees of freedom per node, and translations in the nodal x, y, and z directions. The element may have any

spatial orientation. Solid95 has plasticity, creep, stress stiffening, large deflection, and large strain capabilities, and this model has options such as a prism shape (Fig 2.2). This model represents the pipe shape better than a tetrahedral element does. However, the number of nodes in each element is twice as much as Solid187, hence using Solid95 takes much more time than using Solid187 **[10]**. Table 2.4 shows the number of elements for each mesh size for Solid 95.

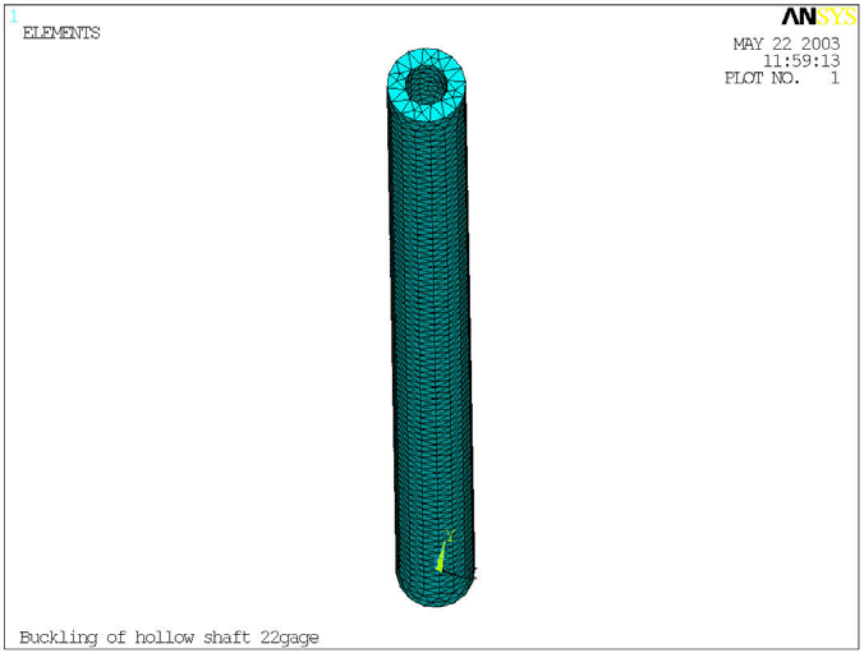

Fig 2.1: Model of simple compression (mesh size=0.15mm)

Table 2.4: Mesh sizes and number of elements for Solid95

Mesh size (mm)	0.15	0.12	0.09
Number of elements	7346	10801	23607

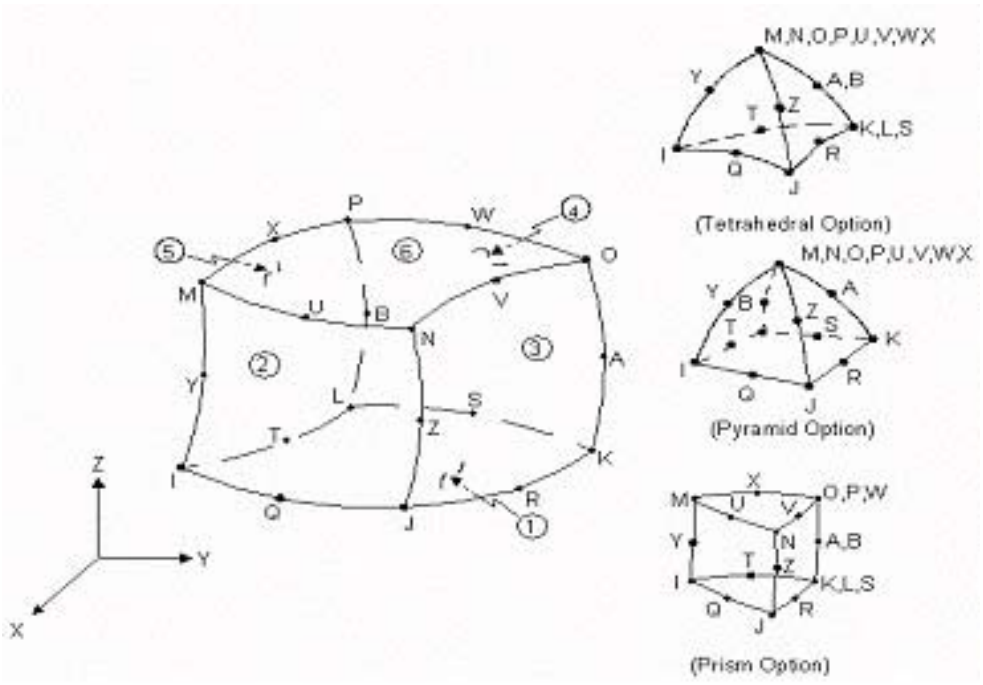

Fig 2.2: Solid95 element [10], a prism option is useful to mesh cylindrical shape.

2.2.1.2 BOUNDARY CONDITION AND LOAD

The procedures presented above are common to all analyses. To consider various boundary conditions, the input of various boundary conditions is required. This section presents the boundary conditions and load settings for the buckling cases considered- fixed-fixed and fixed-pinned.

Boundary and load conditions for fixed-fixed

1. Lower end: Perfectly fixed and cannot move in any direction.
2. Upper end: All the transverse direction movement is restricted. Can move only in Z direction (lengthwise of needle).

3. Load is applied at the upper top area in the form of displacement, equivalent to 1N.

$$Displacement = \frac{L}{AE} = \frac{L}{\pi (OR^2 - IR^2)\, E} = 0.01149\,(mm)$$

where A is the cross-sectional area, OR is the outer radius and IR is the inner radius. Displacement load is used in this analysis because restricting displacement in the Z direction prevents the upper surface from rotating. This simulates the fixed condition with the application of an axial force.

Boundary and load condition for the fixed-pinned

1. Lower end: Perfectly fixed and cannot move in any direction.
2. Upper end: all the nodes of the top surface are restricted to move in the Z direction or symmetrically about the center of the upper surface to ensure a rotational degree of freedom.
3. 1N of load is applied on the upper surface in the form of pressure.

$$\Pr essure = \frac{1}{A} = \frac{1}{\pi (OR^2 - IR^2)} = 3.620\ (MPa)$$

A pressure load is used in this analysis to simulate the rotation-permitted condition; the pressure load is applied perpendicular to the upper surface. Therefore the upper surface can rotate in any direction. A total of 1N is applied to the upper surface for all the analyses. The reason for this will be explained in next paragraph. The APDL (Ansys Programming Design Language) code list is in Appendix 2.1.

2.2.1.3 BUCKLING ANALYSIS [11]

The analysis of buckling using Ansys is not different from other static structure analyses, except several analyses are appended to obtain the buckling solution after performing a static analysis. Here is a conceptual explanation of buckling analysis. First, simple compression analysis is performed. From this analysis, the stiffness matrix of the system is obtained. This matrix is expanded using Lanczos' method algorithm in Ansys in order to find singularities. Each of these singularities represents a mode of buckling. Ansys outputs the mode shape and its critical load as a form of load factor for an initially given load. That is why 1N of load is chosen as the initial load applied to the needle. This means that the load factor can be read directly as the critical buckling load of that structure. Ansys can find other mode shapes and their critical loads. However, for this analysis, the first mode of buckling is the most important here. Analysis is restricted to the first mode shape.

2.2.1.4 RESULTS

Fig 2.3 and Fig 2.4 show the Ansys postprocessor view of the deformed shapes for each boundary condition, and Table 2.5 shows detailed results. In addition to this, Fig 2.5 and Fig 2.6 show the convergences of the analyses. As shown in Table 2.5, analyses of fixed and pinned conditions show good convergence and only small differences from the analytical solutions. Interaction between the skin and needle tip is not considered in these solutions. Hence, these results give only an approximation of the real situation. In the next section, friction will be included.

Table 2.5:Critical Buckling Load of 22 gage needle

	P_{crit}(TH) (N)	Mesh size (mm)			Converge (N).	Difference (%)
		0.09	0.12	0.15		
Fix-Pin	5.725	5.548	5.546	5.547	5.548	3.10
Fix-Fix	11.193	10.659	10.662	10.666	10.655	4.81

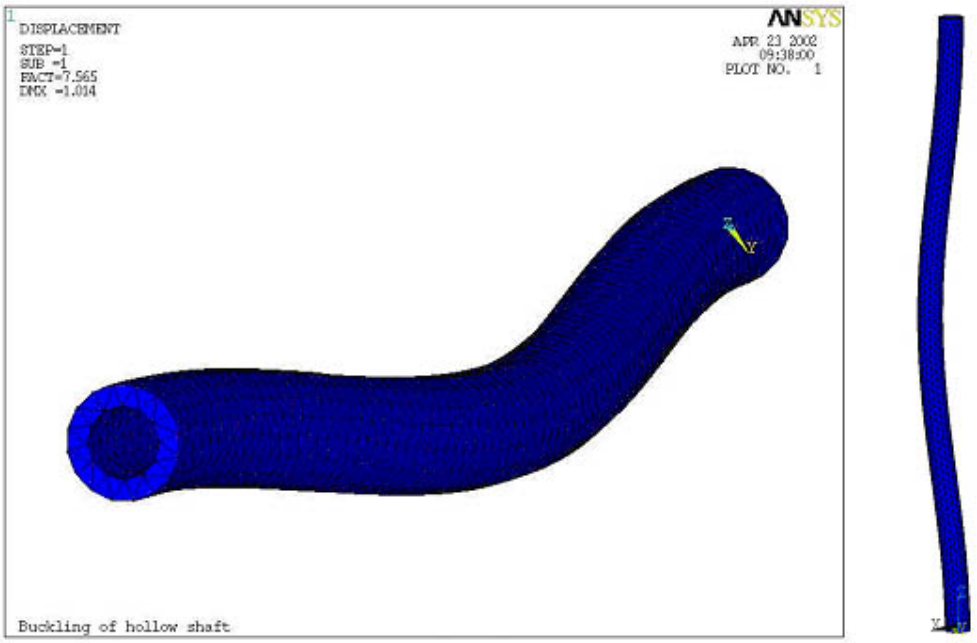

Fig 2.3: Buckling of 22 gage needle (Fixed-fixed condition)

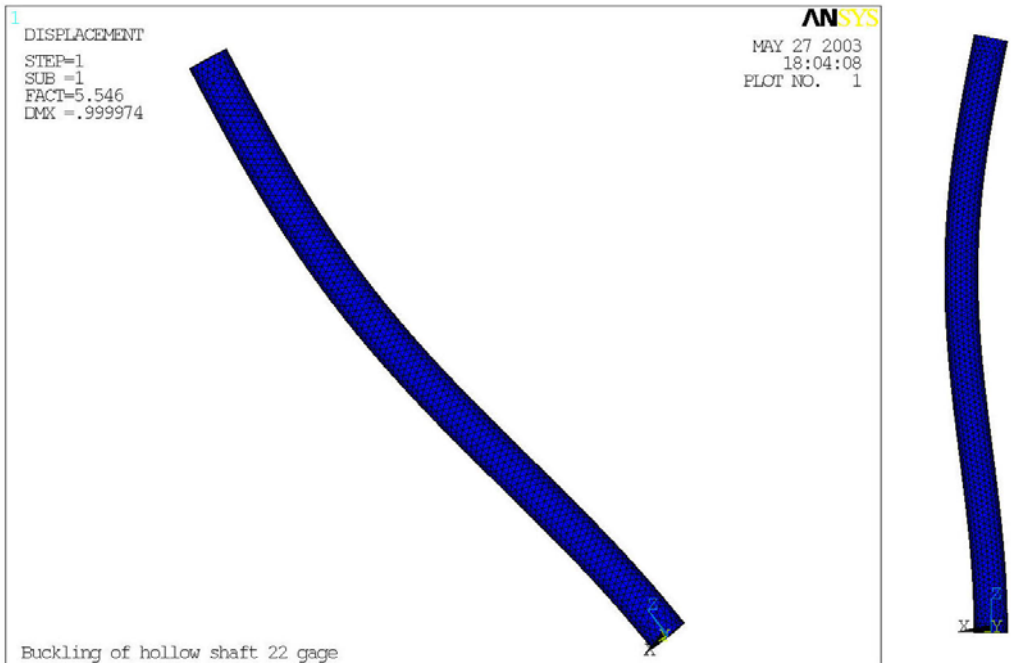

Fig 2.4: Buckling of 22 gage needle (Fixed-pinned condition)

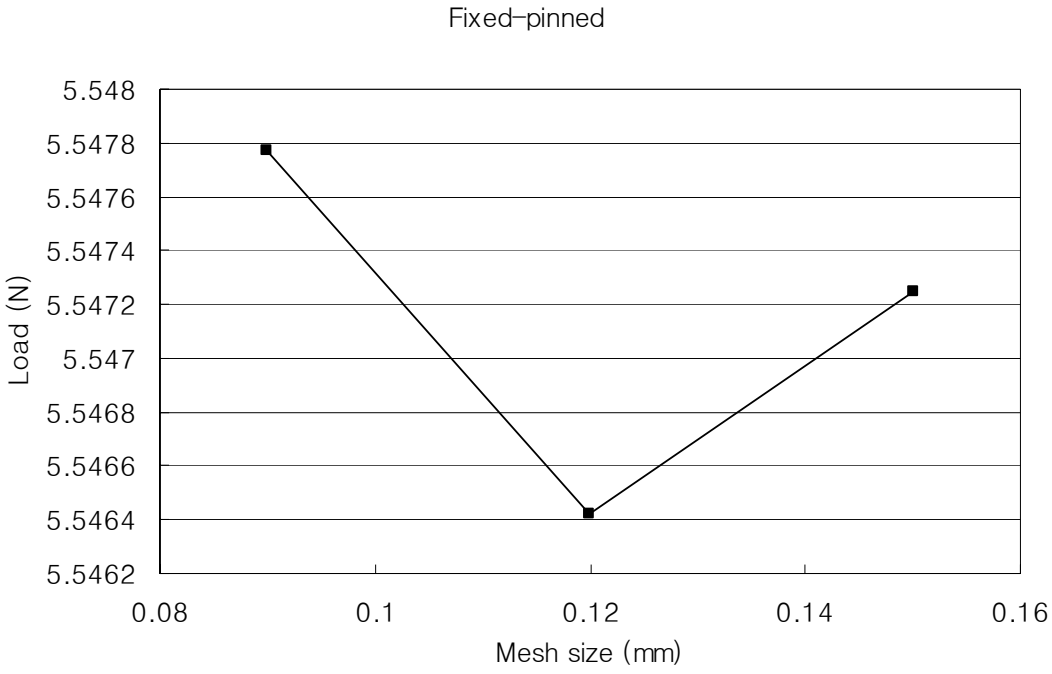

Fig 2.5: Fixed-pinned Buckling Analysis

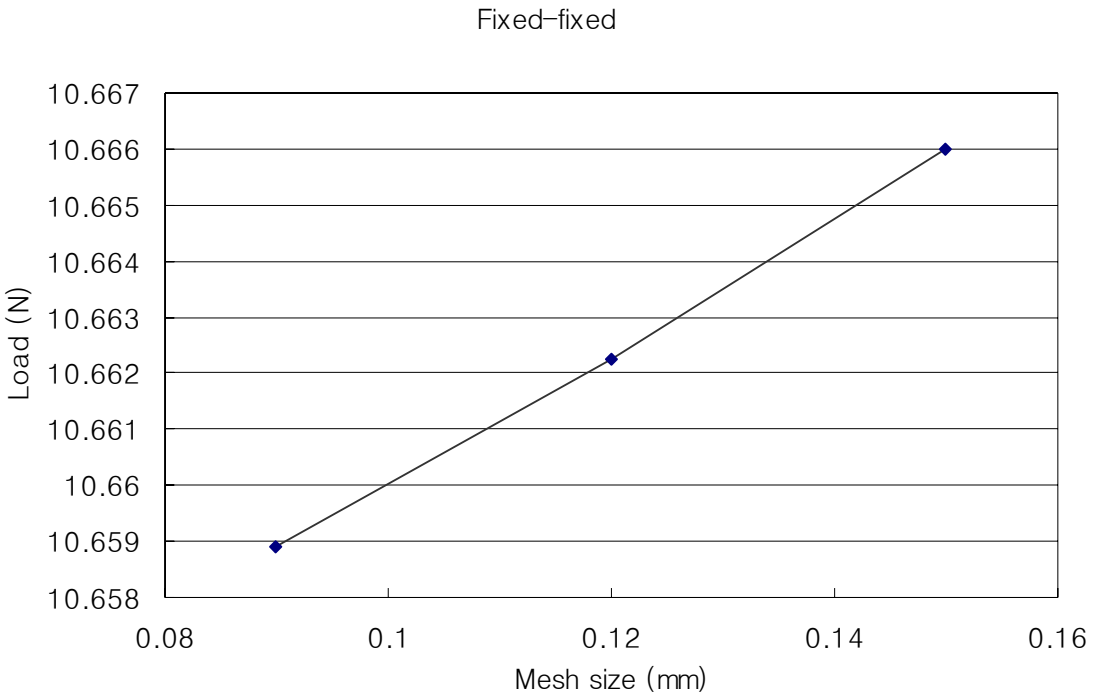

Fig 2.6: Fixed-fixed Buckling Analysis

2.2.2 BUCKLING WITH FRICTION

In this analysis, a more detailed model is introduced. The needle is more like the needles that were fabricated. To consider the interaction between skin and needle, a skin model is introduced. In this chapter, the poking of a flat tube against the skin model and a rigid metal plate is considered.

Poking a flat needle against a rigid surface can reveal boundary conditions for buckling induced by friction. A rigid surface is not deformed, so no depressed area that can hold the needle can be formed during poking. Hence, only the friction effect can be

seen. The analysis of the skin poking model gives the contour of strain. By knowing maximum elongation of skin, the penetration force can be obtained.

2.2.2.1 MODELING & CONTACT MODELING

To make the model more realistic, changes were needed in the analyses, as follows:

1. The upper section of the needle model is thicker so that it is similar to the real needles made in Chapter 3.
2. To simulate the poking situation, the upper end is made rigid.
3. The bottom end is free and a contact element is added to simulate friction between the skin and needle tip.

Fig 2.7 is a conceptual sketch of the simulated condition. This figure shows the boundary conditions for loading. Force is applied to the top surface in the form of pressure to get 1N of force. The side of the top is allowed to move only in the Z (lengthwise) direction. These conditions make it a fixed boundary condition. The poking target is fixed at the bottom in all directions.

The mesh size for the needle is 0.2mm, and meshes near the contact are refined further to get a more accurate solution. The poking target is modeled as a steel plate (E=200GPa). It has a 0.25mm size mesh with refinements near the contacting surface. The model after meshing is shown in Fig 2.8. Dense meshes can be seen near the contact area.

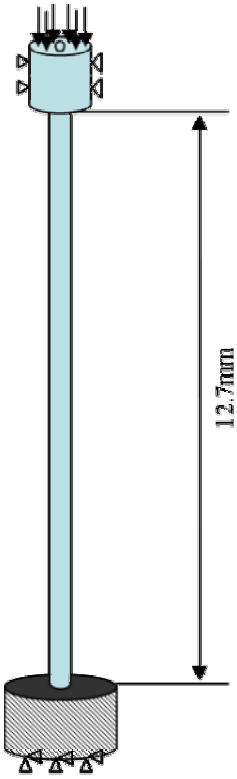

Fig 2.7: Poking Simulation

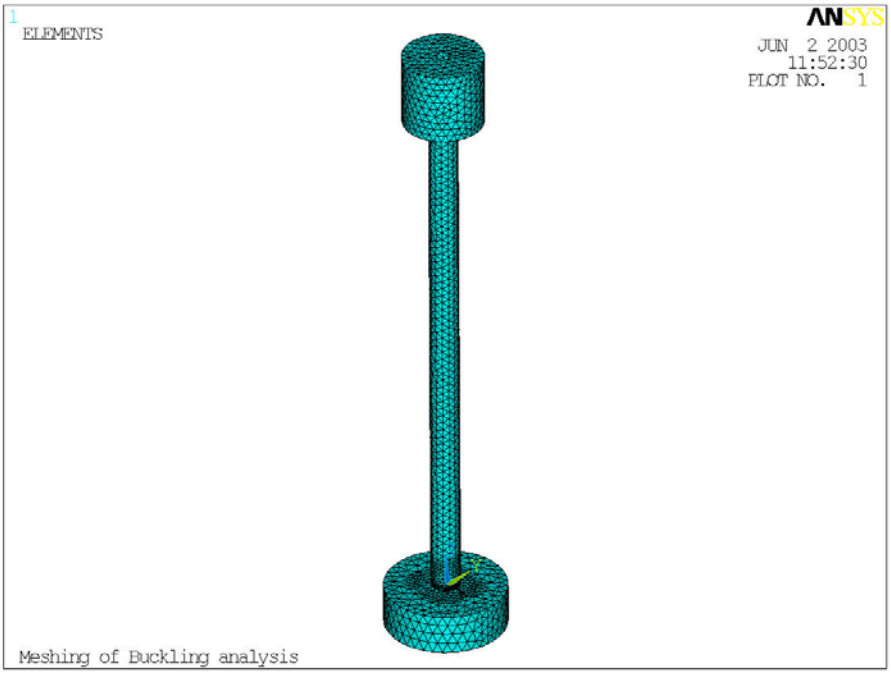

Fig 2.8: Meshing of Analysis

To define the boundary conditions of the lower end of the needle, the simulation of friction at the skin-needle contact is important. In this analysis, contact simulation was performed by the contact elements provided in Ansys.

The contact condition was set automatically by the contact simulation wizard in Ansys. The friction coefficient between contacts is 0.26 (Steel-Nylon6 **[12]**). To find the effect of friction on the boundary condition of buckling, various friction coefficients (0.0, 0.025, 0.05, 0.15, and 0.26) were used. Other conditions are the default settings in Ansys.

2.2.2.2 RESULTS

First, before considering buckling, stress and strain contours can be drawn from the nodal results. Fig 2.9 and Fig 2.10 show contours of stresses along with the deformed shapes. For visualization purposes, only one quarter of the model is shown. A very small stress and almost no deformation can be seen in the steel. Stress concentrations can be seen at the top and bottom of the needle.

The results of the buckling analyses for various μ are shown in Table 2.6. The results are very similar to the results of the Fixed-Fixed buckling analysis shown in Table 2.5, except for the frictionless (μ=0) case. This means that the needle does not slide during poking against a steel plate with friction. Fig 2.11 shows the buckled shape when μ=0.26.

Table 2.6: Critical buckling load with respect to μ

Friction coefficient	0	0.025	0.05	0.15	0.26
Critical buckling load (N)	2.69	10.39	10.39	10.40	10.40

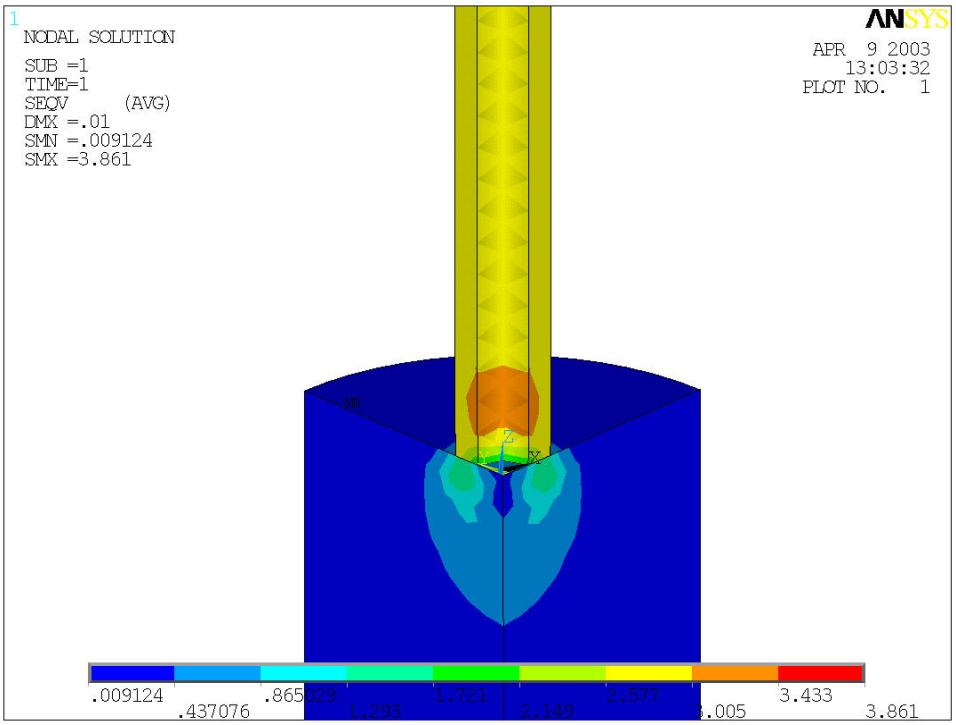

Fig 2.9: Stress Contour of Needle-Steel plate interface

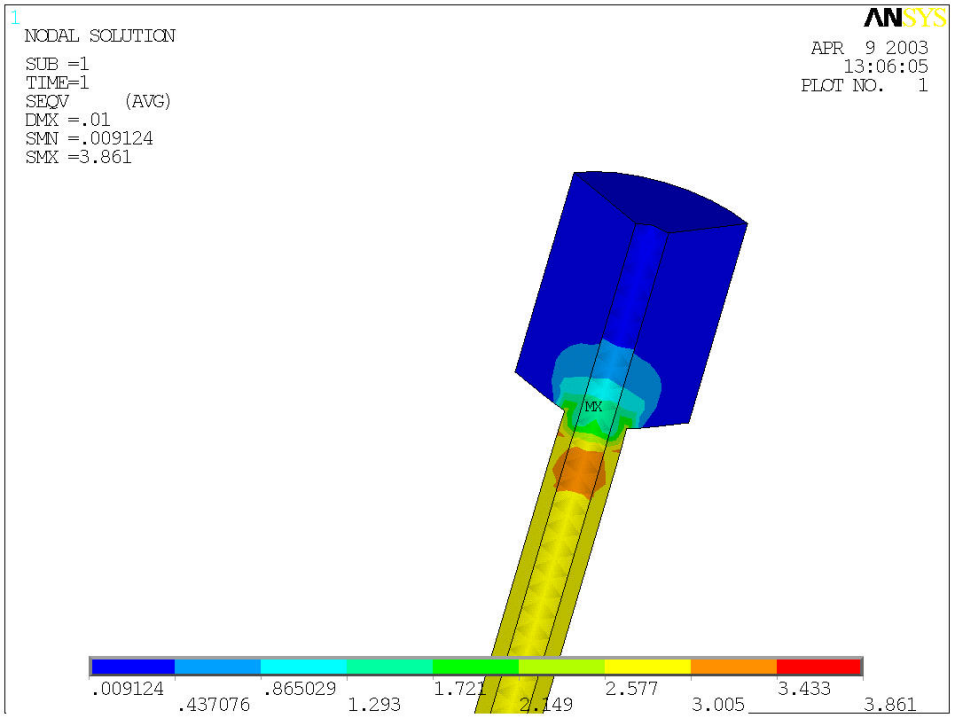

Fig 2.10: Stress Contour of near the needle root

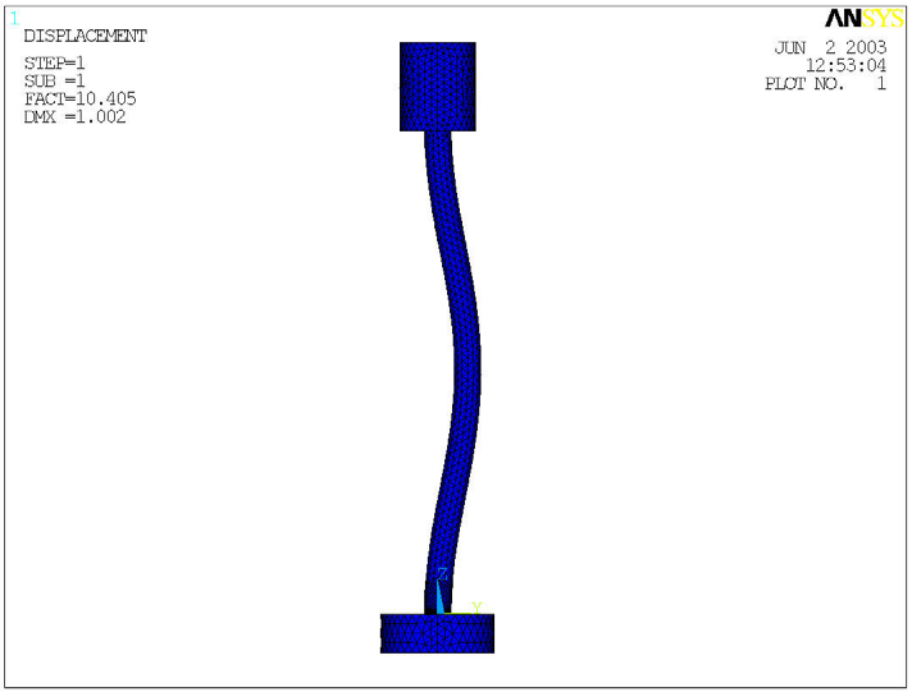

Fig 2.11: Buckled shape of a needle poking against steel plate

2.2.3 SKIN PENETRATION SIMULATION

To simulate poking a plastic needle against real skin, a model is introduced to represent human skin. The poking of skin with a plastic needle is then analyzed. This analysis shows the deformation of skin. By knowing the ultimate elongation of skin, we can determine if penetration has occurred.

2.2.3.1 MODELING

Human skin is a complex tissue consisting of several distinct layers, each consisting of its own components and structure. Skin behaves as a non-homogeneous, anisotropic,

non-linear, visco-elastic material subjected to a pre-stress. Because of the difficulty in testing each layer of human skin in vivo, only data of full skin in vitro are mostly available. The only accessible data of mechanical properties of each layer of human skin are from the model used by Hendricks **[13]**.

Table 2.7 shows a schematic view and the layer thicknesses of human skin. A model consisting of multiple disks is introduced to simulate this complex structure. This simplifies the actual structure into a four layer structure. To use this model in the analysis, data about mechanical strength are required. Mechanical properties of human skin are very different from person to person, age to age, and so on. From Hendricks **[13]** and Oomens **[14]**, mechanical properties of skin can be found and are used in the skin model. Table 2.8 shows the thickness and Young's modulus used in modeling human skin. One notable thing can be seen in the table is that the outmost and thinnest layer, Stratum Corneum, has remarkably higher modulus (1000 times stiffer) than other layers. This is because this layer contains dead cells (dried or cutinized) and dirt.

Table 2.7: Cross-section of human skin (Volar forearm) [13]

Name	Thickness	
Stratum Corneum	0.01~0.02 mm	
Living Epidermis	0.03~0.13 mm	
Dermis	1.1 mm	
Subcutaneous Fat	1.2 mm	

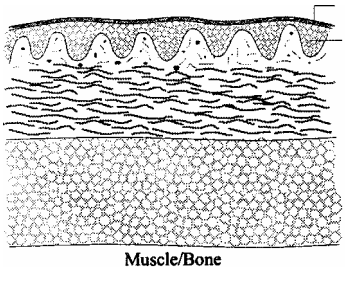

For a boundary condition, the skin is fixed at the bottom, simulating rigid bone. To save computational resources and time, simulation of poking skin is performed using a 1/4 model with symmetric boundary conditions (Fig 2.12). This quarter model also has the advantage of easy visualization. For meshing, the smart mesh size determination function in Ansys is used to save computational resources while maintaining the accuracy of the analysis. To get more detailed results, a mesh refinement function is used for critical sections, such as contacting areas. For example, the Stratum Corneum layer is such a thin and remarkably stiff layer that very dense meshing is necessary. Fig 2.13 shows the detailed meshing of the Stratum Corneum layer. For loading, pressure loading was applied to the top surface, giving a 0.1N force application because the skin model was much weaker than the target used before.

Table 2.8: Mechanical properties of skin model [13], [14]

Name	Thickness (mm)	Young's modulus (MPa)
Stratum Corneum	0.02	12000
Living Epidermis	0.13	16
Dermis	1.1	12
Subcutaneous Fat	1.25	20

Fig 2.12: 1/4 modeling of needle-skin poking

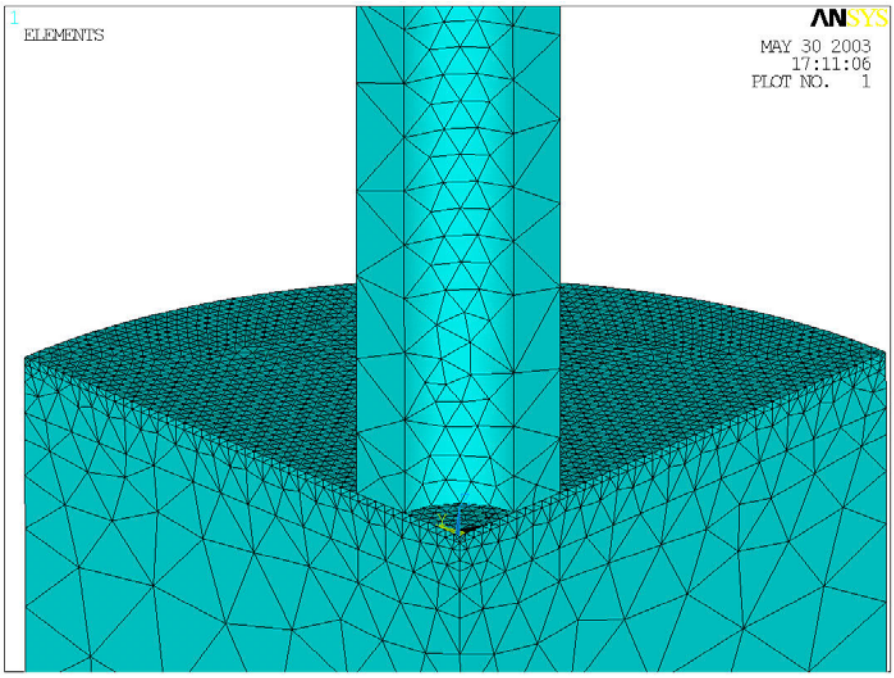

Fig 2.13: Detail of contact section of Fig 2.12

2.2.3.2 RESULTS

The von Mises strain contour and the deformed shape are shown in Fig 2.14. Due to the stiffness of the Stratum Corneum (SC) layer, the strain is very small. All the strain is concentrated at the outer edge of the needle and beneath the SC layer, especially in the dermis layer. Furthermore, skin deformation surrounds the tip of needle with the skin; this produces a fixed-fixed contact surface condition. As can be seen in von Mises stress contour of the skin model in Fig 2.15, all the stress is concentrated on the surface, which has a higher modulus. From the nodal solution, the maximum stress, 26.0 MPa, is read at the node in the SC layer and most common value can be read in that maximum stressed region is around 18.5 MPa. Noting that 0.1 N (for pressure 33kPa) has been applied to the top of the needle, the stress concentration factor is higher than 560.

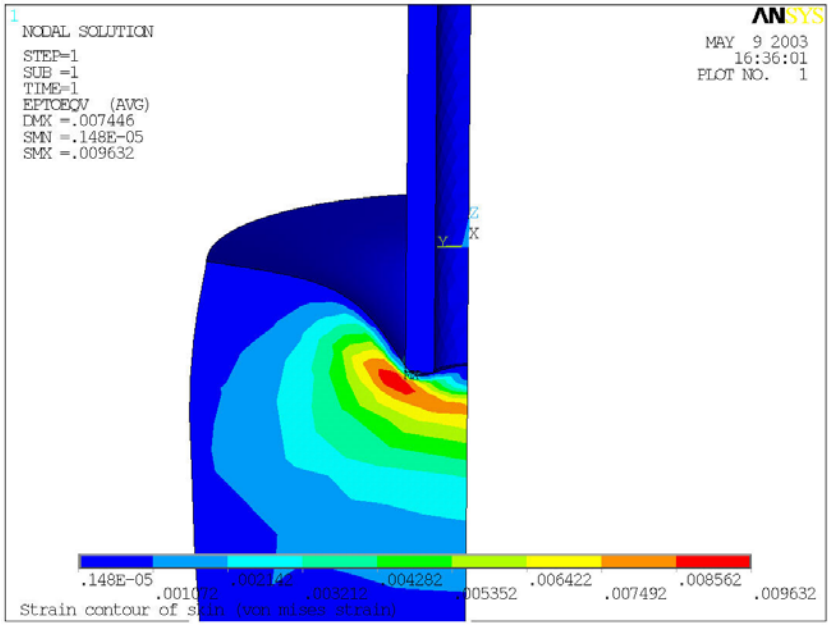

Fig 2.14: Strain (von Mises) contour of skin model

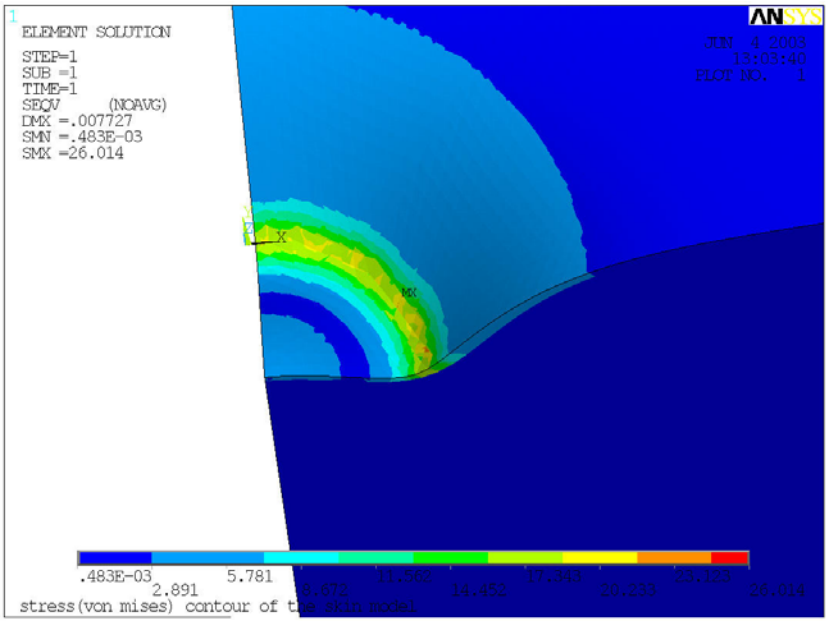

Fig 2.15: Stress (von Mises) concentration on the Stratum Corneum

2.2.3.3 PENETRATION OF SKIN

As mentioned in the previous section, the mechanical properties of human skin differ from person to person, age to age, gender to gender, and even part to part of the human body in the same person. Mechanical data of human skin are very limited, but Davis [15] found the main factors which govern the penetration force of skin to be the interfacial area of the tip and skin, in other words, the insertion force is proportional to sharpness (surface area) of the tip. In his research, for a tip with 10000 μm^2 tip area (0.1mm * 0.1mm), around 1.2 N force is required to penetrate actual human skin (at proximal base of a knuckle, 20 to 26 old, Caucasian male). According to the results of the analyses presented above, a 22 gage plastic cannula does not buckle at 1.2N. If tips can be made with the area that Davis used than such a needle can penetrate skin. This

information is valuable for the further research, such as a guideline for the sharp tip design and the verification of structural capability of the cannulas.

2.3 SUMMARY

A cannula is a thin-walled, concentric, hollow cylinder which, under axial load, may fail in buckling. Analytic and finite element analyses using Ansys are performed to analyze buckling and penetration. For buckling analysis, the buckling behavior of a needle is characterized by a fixed-fixed end boundary condition, assuming that the interface between the cannula and the skin is fixed by the friction. The critical loads that induce buckling failure are obtained by analytical and finite element analyses. For a half inch (12.7mm) length cannula, the critical load is around 11 N (1.2 kgf). This value shows only small (less than 10%) experimental variability.

In addition, a simulation of poking against skin was performed. Based on the papers of Hendriks**[13]** and Oomens**[14]**, human skin is simplified and modeled. From the poking simulation, strain and stress distributions in the skin are obtained. By comparing the ultimate tensile stress and elongation at the failure of each layer of skin, the penetration force can be calculated. Although the properties of skin (tensile modulus, ultimate tensile stress and elongation when failure) differ from person to person, age to age and actual data are very limited, this analysis can be a guideline for penetration force. However from other research **[15]** the insertion (penetration) force is proportional to the interfacial area of tip and skin. This information is valuable for the further researches, such as a guideline for the tip design and the verification of structural capability of the cannulas.

In the next chapter, the fabrication of cannulas from plastics is presented. The design and fabrication of the mold and core structures will be presented, as will injection molding using a micro injection molding machine.

CHAPTER 3

MATERIALS AND FABRICATION

3.1 MATERIAL CONSIDERATION

To produce plastic cannulas successfully, the first thing to consider is the material. In this section, material selection will be considered. The aspects considered are mechanical strength, biocompatibility, and manufacturability.

3.1.1 MECHANICAL PROPERTIES

The tensile modulus of steel is around 210 GPa, but those of plastics are much smaller. This fact hinders the use of plastic materials for needles and has constrained them to be used only as catheters (Fig 1.1). Some properties of commonly used materials are listed in Table 1.1. Mechanical properties of the material used in this research are listed in Table 3.1. The tensile modulus is a measurement of stiffness and is an important factor when determining buckling behavior. Yield strength provides a guideline for design. Failure strength gives good guidance for the maximum load. Crystallinity represents the micro-structure of the material, which determines behavior during deformation. Amorphous materials tend to be brittle. Yield and breakage tend to occur near each other for these materials. Crystalline materials tend to be tough. They break after yield. Considering breakage problems, crystalline materials are better.

Table 3.1: Mechanical Properties of Needle Material Candidates

Material	Nanocomposite	PS	PMMA	PC
Vendor Name	Honeywell Aegis XA-2908	Chevron GPPS 3600	Atohaas Plexiglas V Grade	GE Lexan 121R-111
Yield strength (MPa)	92	46.9	70.3	62
Break strength (MPa)	89	46.9	70.3	72.4
Elongation at break (%)	6.3	3	6	125
Tensile Modulus (MPa)	4000 (Dry) 2900 (Measured)	3100	3100	2340
Crystallinity	Crystalline	Amorphous	Amorphous	Amorphous

Because the tensile modulus is a critical factor in buckling, the nanocomposite material is the best choice. The matrix material of the nanocomposite is nylon 6, whose tensile modulus can be affected by humidity. Careful handling of material, such as drying before injection molding, is required. To confirm the tensile modulus of the XM-2908, a tensile test (ASTM-D638) was performed. The measured modulus was found to be 2900 MPa. The reason for this reduction will be explained later in Chapter 5. Details of the tensile tests are presented in Appendix 3.

3.1.2 BIOCOMPATIBILITY

Because these cannulas are the major part of the hypodermic needle, consideration of biocompatibility is necessary. The biocompatibility of polymer materials can be determined by the toxicology of bulk and surface samples. There is a further classification of biocompatible polymer materials; bioimplantable and biodegradable [2]. This classification is determined by the long-term chemical stability in the human body (blood, tissue) and the toxicological consideration of post-degradation products. Some examples of biocompatible polymer materials are listed in Table 3.2.

Table 3.2: List of biocompatible polymer materials

Bioimplantable	Biodegradable
PE (Polyethylene), PP (Polypropylene), Polyacrylates (PMMA, HEMA), Polyamides (Nylons), PTFE (Polytetrafluoroethlylene; Teflon® or Goretex®)	PGA (Polyglycolicacid), PLA (Polylacticacid), Polyphospazenes

Bioimplantable materials are inert. They are not degraded by or toxic to the human body. They can remain in the human body without any harm. Bioimplantable polymers are used in many areas of medicine, from medical devices to artificial organs. Biodegradable polymers degrade into non-toxic materials in the human body. These materials can be tailored to have a desirable degradation time. They are used in drug delivery systems, sutures and so on.

A typical hypodermic injection does not take more than several seconds. For hypodermic needles, either bioimplantable or biodegradable materials will fulfill the biocompatibility requirements. Biodegradable materials are ideal for needles, considering breakage problems. There is no need to take surgical measures to remove broken pieces; they will be degraded and absorbed into body. But, biodegradable materials are much more expensive than bioimplantable materials. This is not suitable for mass production. Hence, bioimplantable materials were chosen for the plastic needles of this research. The manufacturer's data for the materials used in this research are listed in Appendix 1.

3.1.3 MICRO STRUCTURE

Thermoplastic polymers have chain structures. Monomers are connected to each other to make these chains. Composite materials are different in structure. The nano-clay composite used in this research is composed of a matrix material (Nylon6) and a filler (Montmorillonite). The filler, Montmorillonite, is hydrophilic silicate clay, consisting of stacks of platelets. Each platelet is less than 10 Angstroms thick, but over 1000 times that in width. Under the proper conditions and surface treatment, the spaces between these platelets can be filled with the monomer, oligomer, or polymer of the matrix. This increases the distance between platelets, swelling the clay. Clay platelets swollen with polymer are said to be intercalated. If the clay swells so much that it is no longer organized into stacks, it is said to be exfoliated. This procedure occurs during polymerization. Therefore, the filler is completely enclosed with matrix. By combining nylon6 with montmorilonite, the following property improvements were observed [23]

1. 40% higher tensile strength,

2. 68% higher tensile modulus,
3. 360% higher flexural strength,
4. 126% higher flexural modulus,
5. Heat distortion temperature increased from 65℃ (nylon-6) to 152℃.

3.1.4 MANUFACTURABILITY

One of the important material properties in making a cannula is a polymer's melt flow index. To make a cannula, molten plastic should fill a very narrow cavity completely before it freezes. The lower that the viscosity of the material is, the better it will fill the cavity. This property is characterized by the melt flow index (ASTM-D-1238). Table 3.3 shows the melt flow indices of the materials used in this thesis. According to the data in Table 3.3, PMMA is the most viscous material. But in the injection molding of 22 gage cannulas, even PMMA can fill the cavity completely. Hence all the materials are suitable for a cannula from a manufacturing viewpoint.

Table 3.3: Melt flow index of materials [24]

	Nanocomposite	PS	PC	PMMA
Manufacturer & Name	Honeywell Aegis XA-2908	Chevron GPPS 3600	GE Lexan 121R-111	Atohaas Plexiglas V Grade
Melt Flow, Condition G (g/10 min)	4.0	13.0	17.5	3.7

3.2 FABRICATION

A cannula is a simple, concentric, hollow cylinder. To make a mold that produces a cannula is more difficult than for a solid cylinder because of the hole in the cannula. A core has to be placed right in the middle of the cavity and removed from the mold before part ejection. In addition, the inside cavity of the cannula should be as straight and as concentric to the outside wall as possible. This section discusses the design and fabrication of molds including the core mounting mechanism.

3.2.1 DESIGN

A cannula is a simple, concentric, hollow, circular cylinder. A 22 gage cannula (ID: 0.38 mm, OD: 0.71mm) is chosen for this research. Although 25 or 27 gage needles are much more widely used in the medical field, 22 gage was selected for two reasons. First, the fabrication of the mold for higher gages (smaller needles) involves more complex and accurate non-conventional machining. Second, a smaller needle is too small to measure the mechanical properties of interest using the testing device available.

The length of the cannula was restricted by the mold inserts which were circular with a 1 5/8 inch diameter, due to the size of mold base and the heater installed on the mold base. Furthermore, the plastic inlet is located in the center of the mold insert. The maximum length of the needle is hence half of the maximum length available. Spaces for core alignment mechanisms and a manifold (reservoir) for plastic also have to be provided. Ultimately, the length available for a cannula is around one half of an inch. The

proposed dimensions of the plastic cannulas are listed in Table 3.4. A model generated in ProEngineer® is shown in Fig 3.1.

Table 3.4: Proposed dimensions for plastic cannulas

Outer diameter (inch(mm))	0.028 (0.71)
Inner diameter (inch(mm))	0.015 (0.38)
Length (inch(mm))	0.5 (12.7)

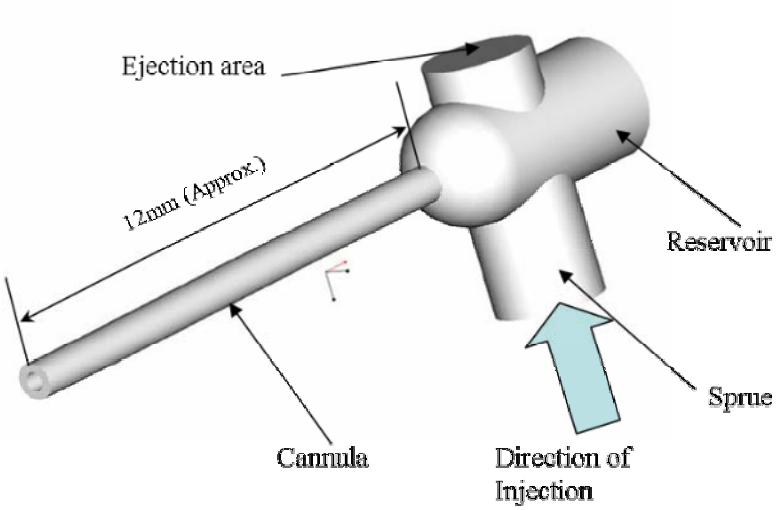

Fig 3.1: CAD Model of Cannula generated in ProEngineer®

3.2.1.1 MOLD DESIGN

A mold is an assembly composed of a mold base, mold inserts, and other accessories. A mold base is an assembly that contains the alignment pins, which align the top and bottom halves of the mold, and the ejection mechanism.

3.2.1.1.1 Mold base

A mold blank (D.M.E. Company, Madison Heights, MI #34R2-7-13) was chosen to fit the molding machine. The mold bottom and top were machined to leave a space to install the mold inserts. Fig 3.2 shows the mold blank and its parts before machining. Fig 3.3 shows the complete assembly.

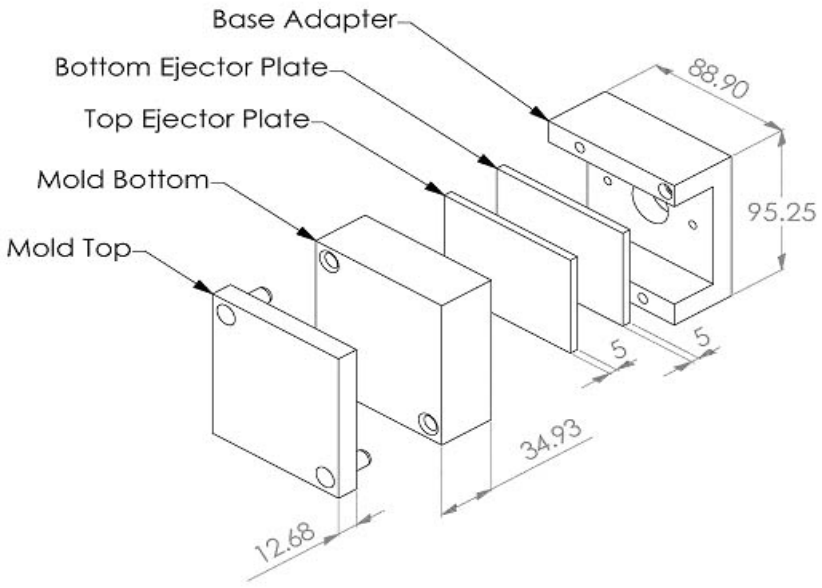

Fig 3.2: Mold blank and its parts before machining (units are in mm)[16]

3.2.1.1.2 Mold insert

Mold inserts provide the cavity to be filled with molten plastic to make a cannula. This cavity makes the outer shape of the cannula. In addition, a core assembly which makes the inner shape of the cannula has to be installed in the mold inserts. Therefore, several requirements should be fulfilled.

1. Cavity

   A cylindrical cavity should be split lengthwise. Otherwise, the mold inserts cannot be separated and a cannula cannot be ejected.

2. Alignment

   As the cavities for the cannula are located on both sides of the mold inserts, both mold inserts should be aligned perfectly to make a cannula with the desired shape.

3. Temperature control

   The wall of a cannula is very thin (around 0.18 mm). When a long cannula is made, molten plastic can freeze before reaching the end of the cavity; this situation is called a short shot. To minimize this failure, the temperature of the mold should be controlled properly.

4. Consideration for core alignment

   A cannula has a hole inside. To make this hole, a core has to be placed right in the center of the cavity. A core alignment mechanism should be attached to the mold inserts as easily and firmly as possible. One must consider the installation of the core alignment mechanism in the mold insert. The design of the core alignment mechanism is considered in the next section in detail.

The alignment of both inserts is achieved by using alignment pins. These pins correct errors that occur during mold making and keep the cross-sectional shape of the cavity circular. To control the temperature of the mold insert, a heater is placed in the mold assembly. In addition, heaters and mold inserts have to be thermally isolated from

the rest of the mold because the mold temperature has a significant effect on a part's quality. To isolate the mold insert and the heater, ceramic insulation plates were used. Fig 3.3 shows the mold assembly.

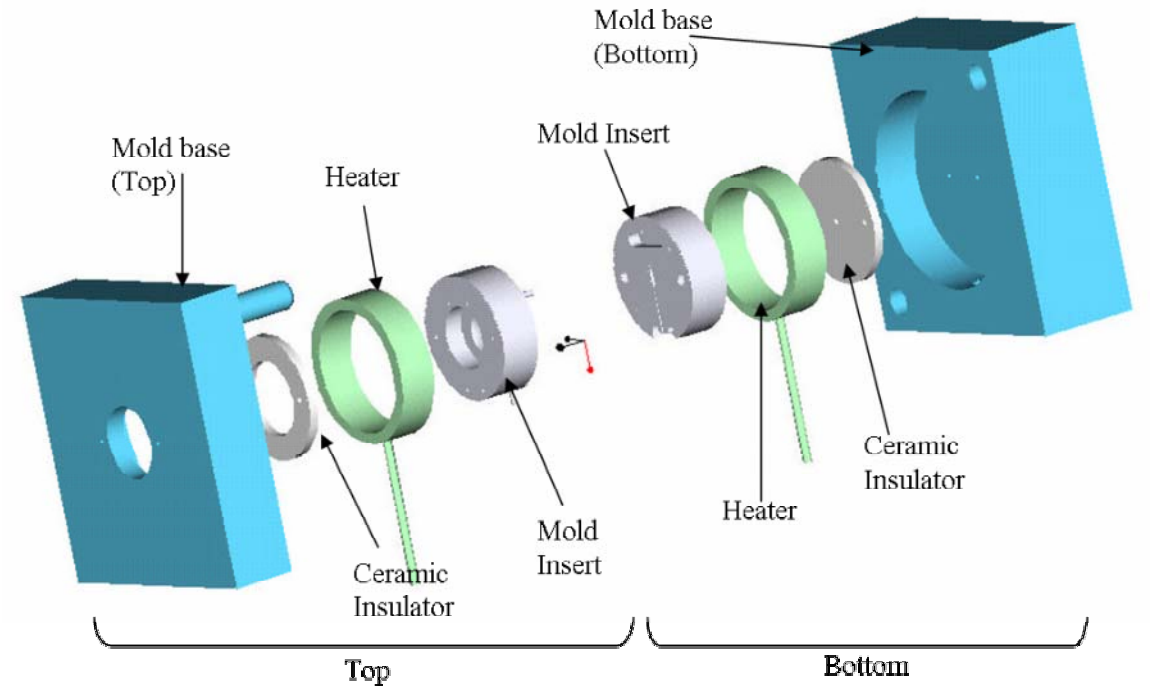

Fig 3.3: Exploded view of machined mold top and bottom assembly

3.2.1.2 CORE ALIGNMENT

When a cannula is made by injection molding, good alignment of the core is necessary to produce a hollow structure.

There are several requirements that the core assembly has to fulfill;

1. Stiffness

   To minimize resistance to the flow of molten plastic, the core is placed perpendicular to the direct injection flow of plastic and parallel to the long flow

direction as in Fig 3.4. This means a core is required to be as stiff as possible to prevent its deflection. Otherwise, it will be very difficult to remove a deflected core without breaking the needle.

2. Concentric alignment

   To have isotropic, balanced properties and to fill the volume of the cavity completely, an accurate core alignment is required.

3. Straight core

   A straight core is needed for the same reasons as for concentric alignment.

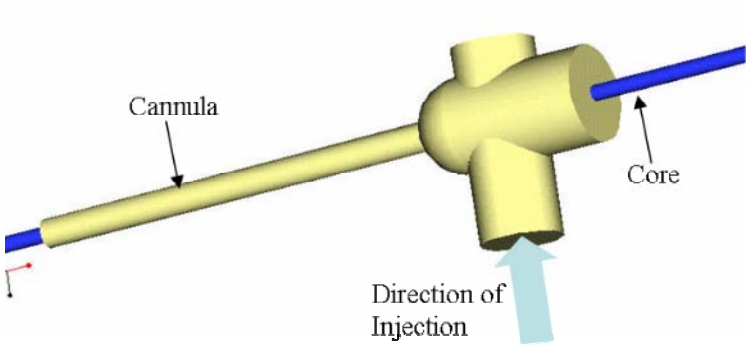

Fig 3.4: Placement of core (Perpendicular to injection direction)

To meet these requirements, several assembly designs were devised. Two materials were tried for the core; SL epoxy acrylate (Stereolithography) and steel wire. More detail about the SL and steel wire cores will be described in the mold making section.

Two alignment designs were considered; V-block and tubular. The V-block design uses V-blocks installed and trimmed in the mold insert to align the core. Fig 3.5 shows a steel wire core stock (the head stock is made of brass) installed in the mold insert with a V-block. Fig 3.6 shows an SL core stock resting in a V-block before installation into the mold insert.

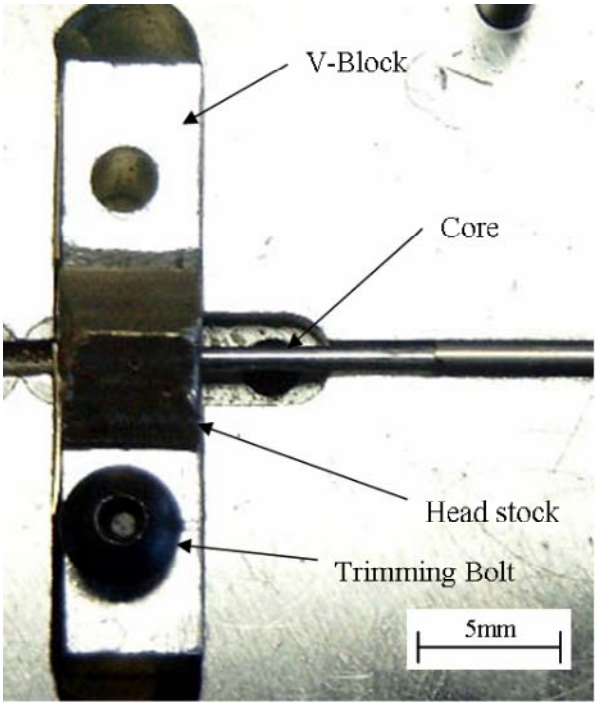

Fig 3.5: V-block and core stock installed and aligned in mold insert

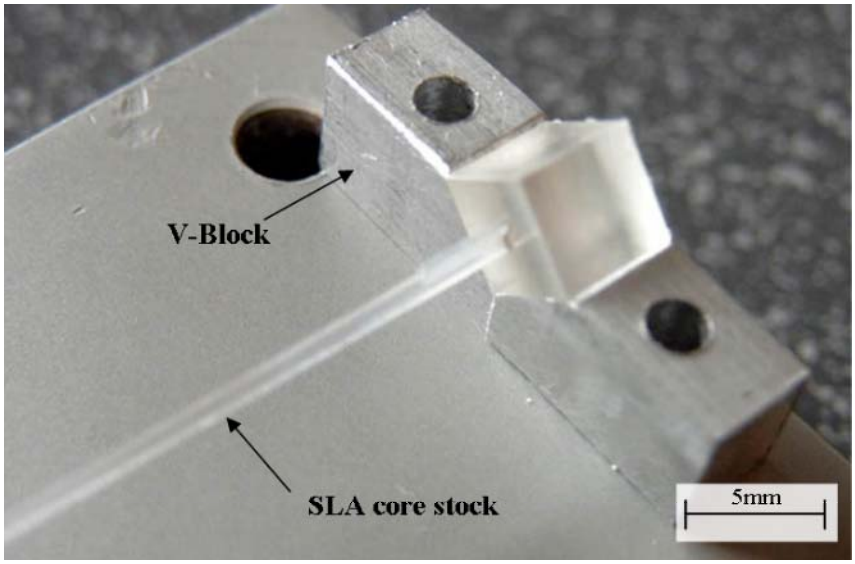

Fig 3.6: SL core stock resting on a V-block before installation in the mold insert.

However, the V-block method does not produce good enough alignment accuracy. For a thicker needle, such as 18 gage (1.27mm OD), it is satisfactory. But it is not

accurate enough for a thin needle, such as 22 gage. Also, it is difficult to hold the core still while injection molding. There is only the friction between the head stock and mold to hold the core in position. Additionally, the seal between the head stock and mold is not good enough, so leakage occurs. Therefore, for needles above 22 gage, the tubular design is used.

A tubular design uses steel wire as a core. Guide tubes are used in both ends to align and seal the cavity. This design requires accurate guide tubes. As described above, the dimensions of the needle in this design is the same as that of an actual 22 gage needle. Small pieces cut from an actual 22 gage needle are used to guide the wire. This design does not require a V-block. The assembly is very simple. Furthermore, cannulas with sharp tips can be made by changing one guide tube at end with a sharp tip cut from a real needle. Actual installation of tubular alignment is shown in Fig 3.7.

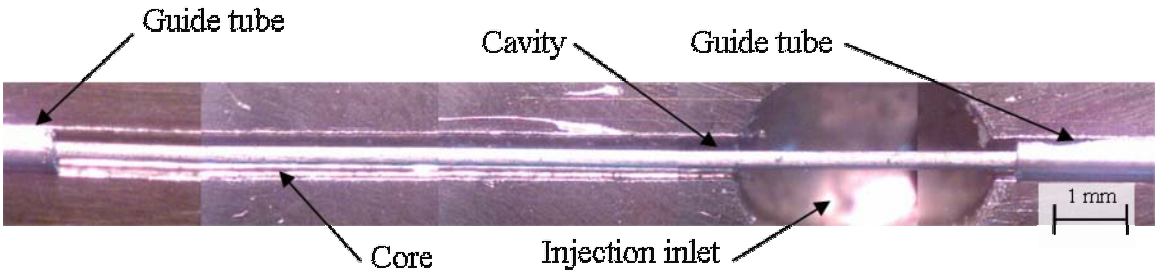

Fig 3.7: Tubular core alignment assembly installed in mold insert

The original tubular design does not include a structure which holds the core assembly during injection molding. There is friction which keeps the core assembly in position during injection molding in the V-block design. In the tubular design, however, there is no friction to hold the assembly in position. Therefore, a harness structure is required. The design requirements for the harness structure are listed below.

1. Functional requirements
    1) It can produce friction that can keep the assembly in position.
    2) Easy to be unlocked if necessary.
    3) Should be simple.
2. Material requirements
    1) Can withstand high temperature.
    2) Should be flexible and easy to cut.

Because the bottom side of the mold moves during clamp closing, a misaligned core assembly at this moment can cause severe damage to the mold insert. A core assembly should be mounted on the stationary side of the mold. However, the cannula sticks to the movable side of the mold. At this moment, the core assembly should be easily detached from the stationary side. Additionally, this harness assembly should be very small so it can fit into mold inserts and should be heat-resistant to endure the high temperatures of the mold insert. To fulfill these requirements, a simple bottle neck design is devised. The harness assembly is made out of Teflon®, which has good flexibility and high temperature resistance. The design of the harness assembly is shown in Fig 3.8. By making the entrance bottle neck shaped, the core stays aligned while clamp is closing. This prevents severe damage induced by a misaligned core. After injection, the core with a cannula can be detached from the mold easily, because the harness structure is made of a flexible material (Teflon®). As shown in Fig 3.8, the harness can be trimmed to control bottle neck size. The final design of the mold insert is shown in Fig 3.9.

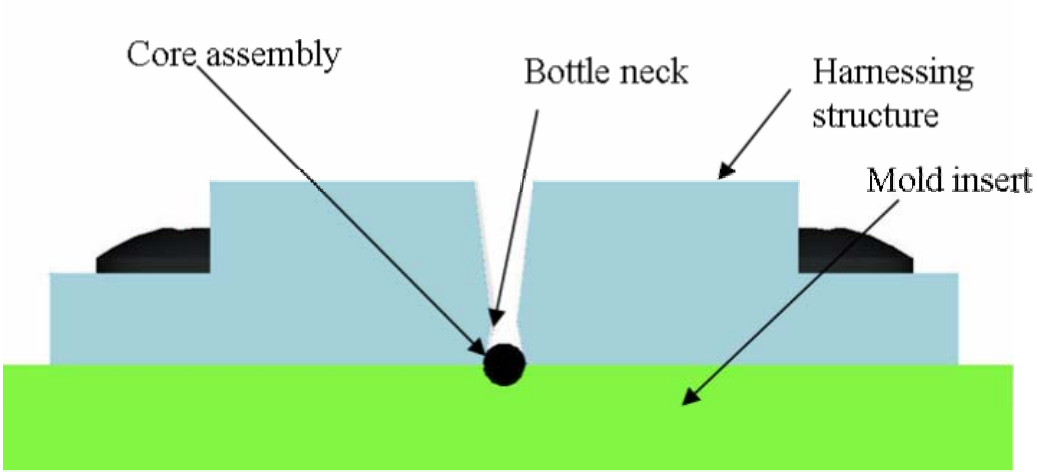

Fig 3.8: Bottle-neck shape core harnessing structure

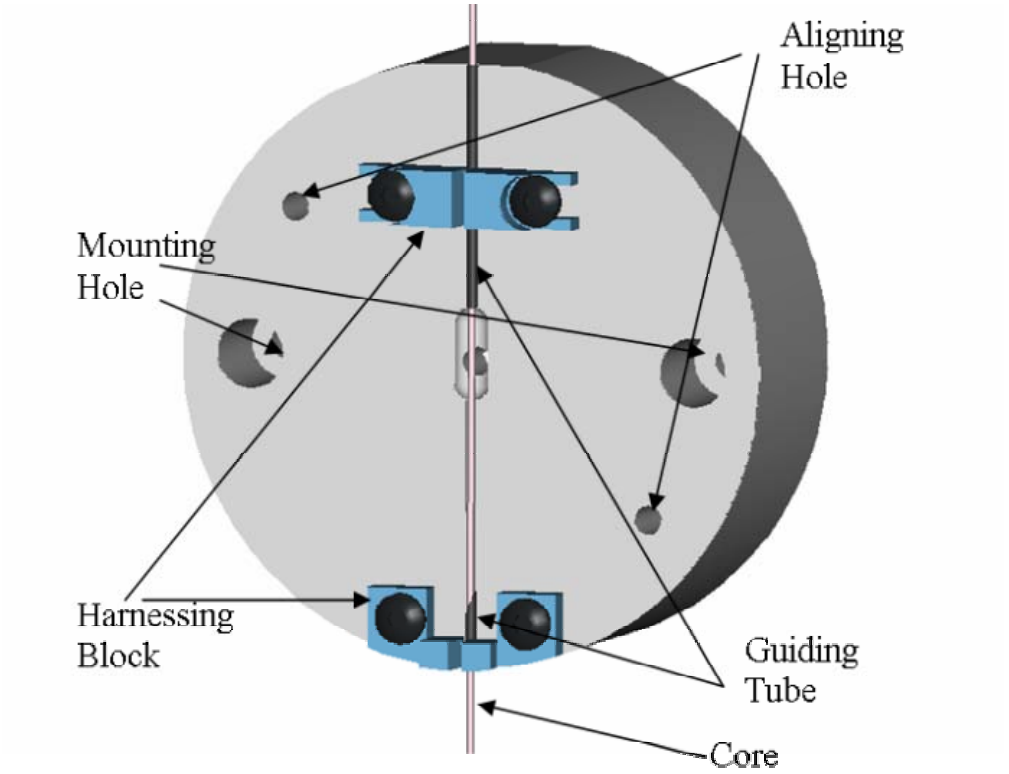

Fig 3.9: Complete assembly of mold inserts (Top)

3.2.2 MOLD-MAKING

Two approaches are tried to make the mold; rapid tooling and conventional machining. Rapid tooling is a simple and fast method of mold fabrication. Mold inserts are made directly from a CAD model using a rapid prototyping machine. The Viper Si2® from 3D Systems (Valencia, CA) in the RPMI is used to make SL molds and other assemblies. Two materials are used for mold materials. They will be considered in the next section. Conventional mold-making is the fabrication of a mold out of metals using machining. This involves various kinds of machining: milling, drilling, and so on. 12L14 low carbon steel is used for conventional mold making. In the next section, detailed considerations of the material and fabrication will be presented.

3.2.2.1 MOLD MATERIALS

For the SL approach, photosensitive polymer materials, RenShape™ SL5510 from Vantico (East Lansing, MI) and WaterClear™ 10120 resin from DSM Somos (New Castle, DE) are used. The mold inserts are made of RenShape™ SL5510 and the core assemblies for V-block are made out of WaterClear™ 10120 resin. Properties of the resins are listed in Table 3.5.

SL5510 is optimized for mass production and high accuracy. Its minimum layer thickness is 0.05mm, which produces an accurate mold. It takes more than four hours to make the mold inserts, which can reduce mold-making time to one third of that of conventional machining. However, SL materials are polymers, and are very weak at high temperatures and under impact. To accommodate these disadvantages, much milder injection molding parameters are tried.

Table 3.5: Properties of SL materials [25][26]

			RenShape™ SL5510	WaterClear™ 10120
Tensile Modulus (MPa)		ASTM D638M	2854	1710
Tensile strength (MPa)		ASTM D638M	66	26
Heat Deflection Temperature (℃)	@ 0.46MPa	ASTM D648M	54	44.9
	@ 1.81MPa		47	46.8
Minimum layer thickness (mm)		N/A	0.05	0.05

For conventional mold making, 12L14 Low-carbon steel was used. This steel contains lead, sulfur, and phosphorus. It has excellent machining characteristics and good ductility, which make it easy to bend, crimp and rivet. It is very difficult to weld and cannot be case hardened. 1-5/8 inch in diameter cold drawn rod was purchased for the raw stock.

3.2.2.2 FABRICATION

3.2.2.2.1 SL (Sterolithography)

SL is a rapid prototyping technology that uses a laser to cure low MW (molecular weight) photo sensitive liquid resin into a high MW solid. This enables complex shapes generated in a CAD program to be realized in a few hours. The SL fabrication flowchart is shown in Fig 3.10.

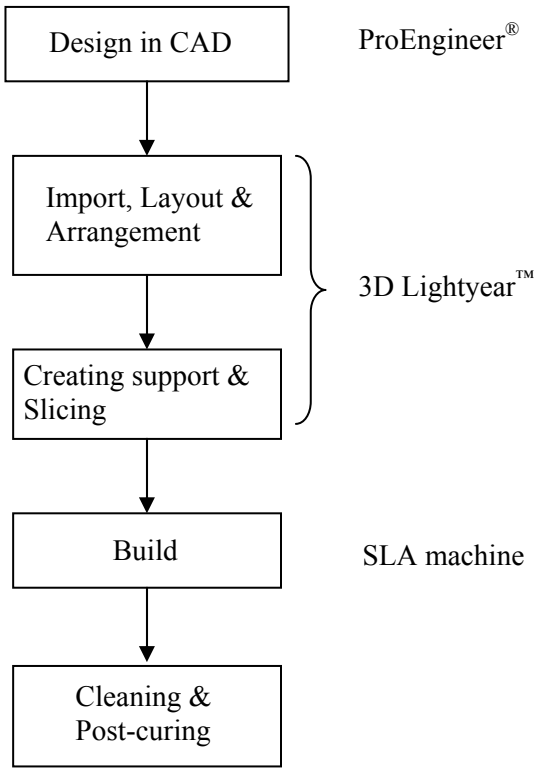

Fig 3.10: Procedure for making a part using SLA

The most critical features in this design are the 0.7 mm diameter arcs. The Viper Si2®(Fig 3.12) from 3D Systems (Valencia, CA, 91355) was chosen because of its high definition capability (minimum feature size 0.05 mm). But this method has several disadvantages. As the SL is a layer by layer process, every curve in Z-X and Y-Z plane is approximated as stair-step shapes at the micro scale (Fig 3.11). In addition, the original material is a liquid. Support structures are required to prevent the part from collapsing and should be built before making parts. Good surface finishes cannot be obtained where the surfaces touch the supports. These supports should be placed on the surfaces that do not contain important features. To minimize errors from shape approximation and supports, the layout and orientation of parts should be determined very carefully.

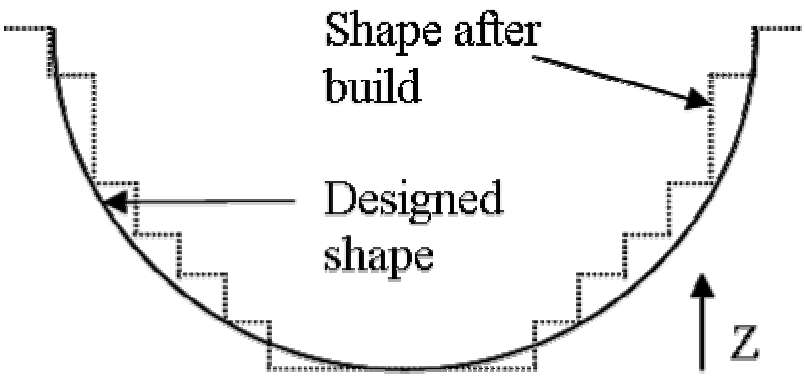

Fig 3.11: Stairstep shape approximation in SLA

Fig 3.12: Viper Si2® SLA machine from 3D Systems (Valencia, CA)

One example of the importance of the layout and orientation of parts can be found in fabrication of the SL core. The model orientation of Fig 3.13 (A) can save build time. However, the very thin core is lying on the support structures. This part cannot be

detached from the supports safely. By changing orientation and sacrificing build time, good core quality can be achieved (Fig 3.13 (B)).

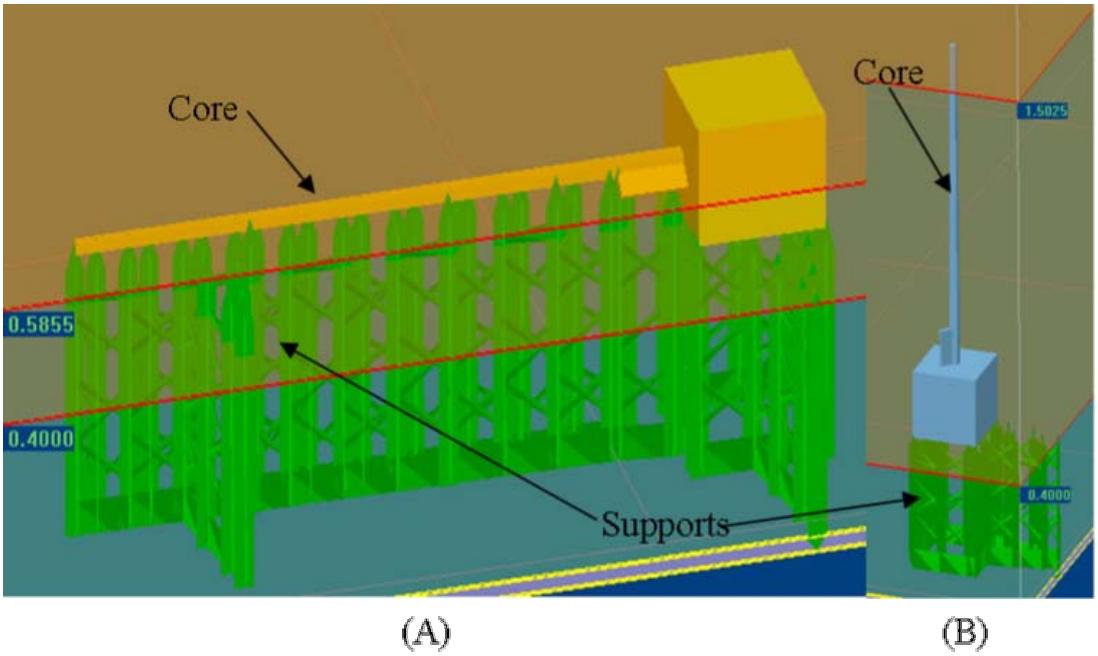

Fig 3.13: Failed orientation (A) and improved orientation (B)

After the part is built in the SLA machine, excess resin is removed with rubbing alcohol and TPM (Tripropylene Glycol Methyl ether). After cleaning, a post-cure process is performed in an UV oven. UV rays cure the unreacted resin trapped inside the shell, and hence enhance the mechanical properties of the parts.

3.2.2.2.2 Conventional mold making

Conventional mold making was performed in the machine shop. Most of the machining was performed in a CNC milling machine. The machining procedure is delineated in Table 3.6. Cutting the groove is a challenging procedure because the size of the groove (0.7mm) is smaller than the smallest ball-nose milling cutter available. Therefore, the groove is cut in a HS3100 WEDM (Wire Electro Discharge Machining)

machine (Machine tools division, Brothers Industry, Ltd) (Fig 3.14). Using 0.01 inch wire, it can cut grooves for cannula sizes up to 25 gage (0.02 inch).

This WEDM machine can cut just enough material to make a small groove for the needle cavity, according to G code program. However, electro-discharge machining usually leaves a poor surface. Because it is a localized heating process, an oxidization layer is left behind. A post process, such as grinding or buffing, is required. In this case, WEDM is programmed to remove so small an amount of material that errors associated with the oxidization layer and deflection of wire are significant. Also, because the groove is concave, it cannot be ground or buffed easily. To correct these errors, manual scraping using a real needle was performed. Because the mold material has excellent machining characteristics, small amounts of material can be cut by hand. A real needle without a tip was used as a tool and a measuring guide.

Table 3.6: Procedure to machining a mold insert

Seq	Procedure	Machine
1	Cut the rod stock to make a raw stock for a mold insert.	Saw
2	Make both faces of the stock flat and smooth.	Mill, Grinder
3	Drill the injection hole and mounting holes.	Mill
4	Grooving (cutting a groove which is half of the cannula).	WEDM
5	Surface finish groove (scraping).	N/A
6	Cutting to make reservoir space.	Mill
7	Cutting the injection entrance on the other side which faces injection nozzle (fixed side of mold).	
8	Drilling to make a hole to mount core-mounting assembly (fixed). Cutting the space to accommodate core mounting assembly (movable).	
9	Install guiding pins (fixed). Drilling to make holes the guiding pins can go through (movable).	
10	Mount core-mounting assembly.	N/A

Fig 3.14:HS-3100 WEDM machine (PMRC machine shop)

3.2.3 INJECTION MOLDING

After fabrication, the mold inserts were installed in the mold base to complete the mold assembly. This assembly was installed in the injection molding machine to make parts. This section considers the equipment, settings, and other parameters associated with injection molding.

3.2.3.1 EQUIPMENT

Injection molding of plastic needles was performed by the Sesame™ .080 Nanomolding™ machine (Fig 1.3). Table 3.7 shows the specifications of the molding machine.

Table 3.7: Specifications of Sesame™ .080 Nanomolding™ machine

Maximum injection volume	0.082 cubic centimeters
Maximum injection	50,000 psi
Clamping capacity	810 pounds (@ 90 psi air)
Ejection capacity	50 pounds (@ 90 psi air)
Clamp stoke	6 inches
Injection speed (maximum)	1000 mm/sec

Some important parameter settings for molding a 22 gage cannula are shown in Table 3.8. Other parameters follow machine defaults. These parameters are optimized for the material of the mold inserts. For the SLA mold inserts, much milder injection parameter settings are used, considering its weak mechanical properties.

Table 3.8:Injection parameters for each mold insert

	Metal mold inserts	SLA mold inserts
Mold cool time (sec)	5	1
Injection speed 1 (mm/sec)	1050	200
Maximum pressure (Bar)	1500	400
Holding pressure 1 (Bar)	2000	400
Holding pressure 2 (Bar)	1500	300

3.2.3.2 SET-UP

For each plastic material, the recommended temperatures for the barrel, nozzle and mold are different. Up to a certain limit, a higher temperature is better because the

viscosity of molten plastic decreases exponentially with the temperature. But higher temperatures also mean easier degradation. These environmental specifications are summarized in Table 3.9 and Table 3.10.

3.2.3.3 PART PRODUCTION

Cannulas were made by injection molding. Four materials (PS, PMMA, PC, Nano-composite) were tried. For preparation, material pellets were dried. This is one of important procedures to do before injection molding. For materials which show hydrophilic properties, moisture in atmosphere tends to be absorbed and disrupt the chain structure of polymer by hydrolysis reaction. This will reduce the quality of the parts made.

PS shows hydrophobic properties, thus it was used directly in injection molding process without drying. The nanocomposite material was dried more than 1 hour in oven at 80℃ and was packed in airtight container with desiccant (Silicate) pouch. Other materials (PC and PMMA) were used directly without drying.

For a injection molding to make needles, Table 3.9 shows suggested temperatures for each material. For each case, mold and machine parameters follow the data listed in Table 3.8 and the temperature used in plasticizing block and nozzle follows the data mentioned in Table 3.10.

However, SLA mold inserts cannot endure the heat and impact of the nozzle. After the first several shots, the inlets of the mold inserts were severely deformed and the cavity was broadened (Fig 3.16). Molten resin melts and broadens the groove and infiltrates the gap between the mold inserts and deforms the cavity, resulting in dull edges. Fig 3.15 illustrates this.

Table 3.9: Suggested temperature conditions for each material [24]

Property	Nanocomposite	PS	PC	PMMA
Suggested Nozzle Temperature	470-490 °F (246.1-254.4 °C)	425 °F (218.3 °C)	530-570 °F (277-299 °C)	410-482 °F (210-250 °C)
Suggested Block Temperature	480-500 °F (248-260 °C)	400-415 °F (204.4-212.8°C)	540-580 °F (282-304 °C)	392-446 °F (200-230 °C)
Suggested Mold Temperature	180-200° F (82-93° C)	150-170 °F (65.69-76.7°C)	160-200 °F (71.1-93 °C)	160 °F (71.1 °C)
Glass Transition Temperature	140 °F (60 °C)	194-212 °F (90-100 °C)	150 °F (302 °C)	194-212 °F (90-100 °C)

Table 3.10: Actual temperature condition used for making cannulas

PROPERTY	Nanocomposite	PS	PC	PMMA
Nozzle Temperature	480°F (248.9°C)	430°F (221.1°C)	530°F (276.7°C)	510°F (265.6°C)
Block Temperature	485°F (251.7°C)	435°F (223.9°C)	535°F (279.4°C)	515°F (268.3°C)
Mold Temperature	200°F (93.3°C)	120°F (48.9°C)	200°F (93.3°C)	160°F (71.1°C)

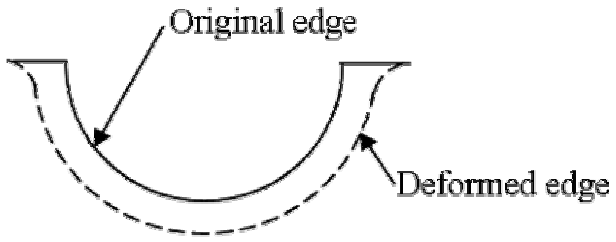

Fig 3.15: Cross-sectional view of deformed SL mold inserts

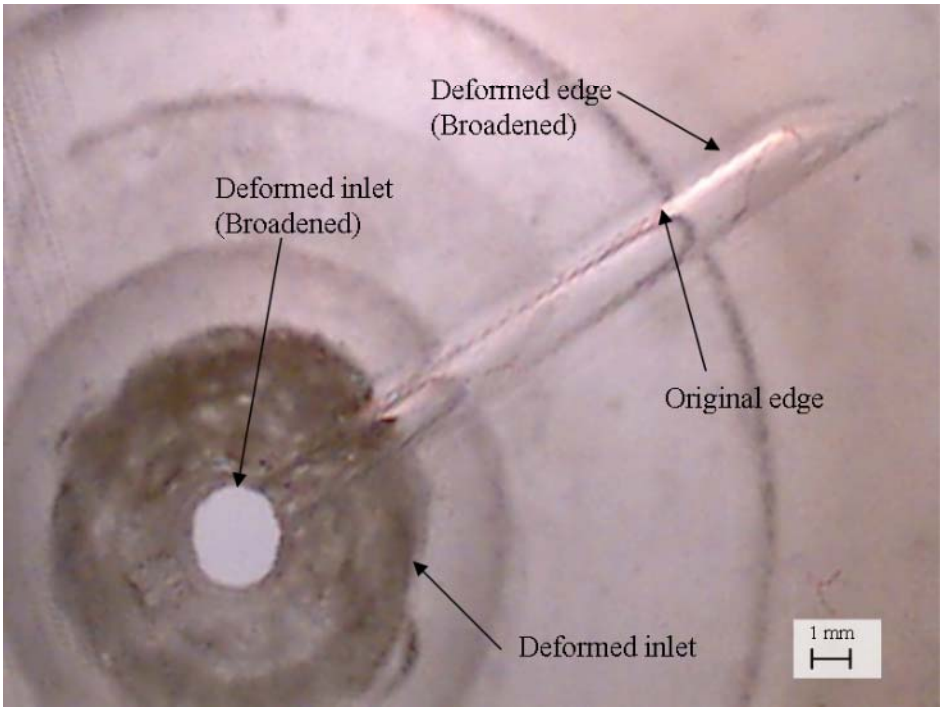

Fig 3.16: Deformation of SL mold insert (after several parts have been made)

Because of this, only metal mold inserts were used to make cannulas. Around 100 cannulas were made. Fig 3.17 shows a nano-composite cannula before core removal, Fig 3.19 shows a polystyrene cannula. For the cannula in Fig 3.19, a tip cut from a metal hypodermic needle was used as the core guide tube. However the sharpness of tip is not so good for the plastic cannula, because the reverse shape of the sharp tip is produced in the plastic parts (Fig 3.18). To enhance the sharpness, making the guide tube with the reverse shape of needle tip is needed.

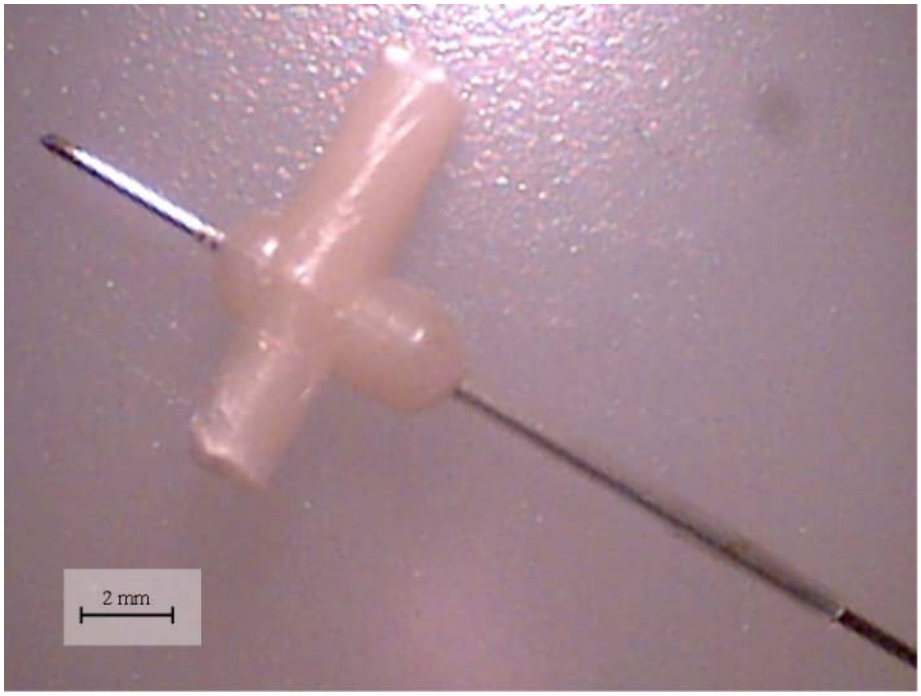

Fig 3.17: Nanocomposite cannula with core

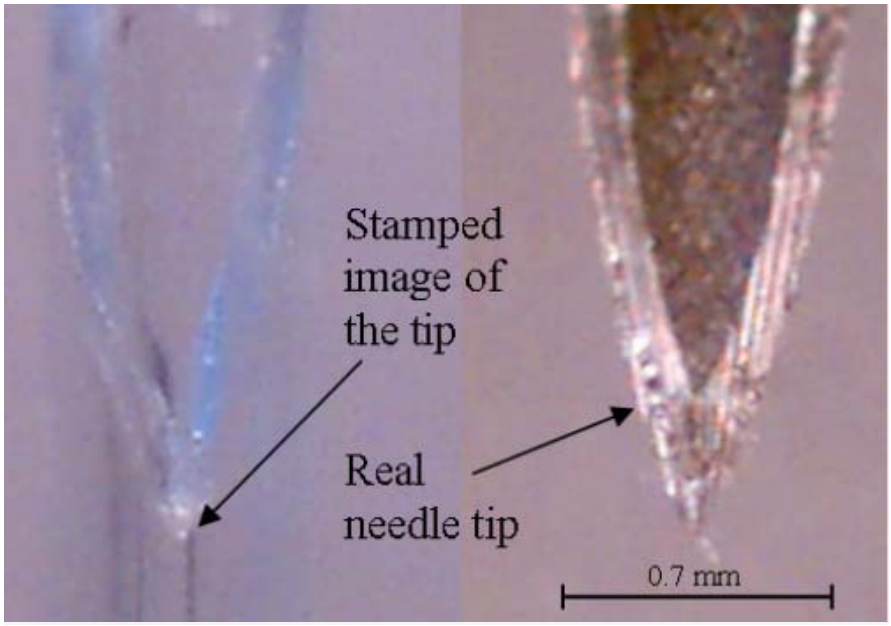

Fig 3.18: Tip of the cannula (Left: PS cannula, Right: Real hypodermic needle)

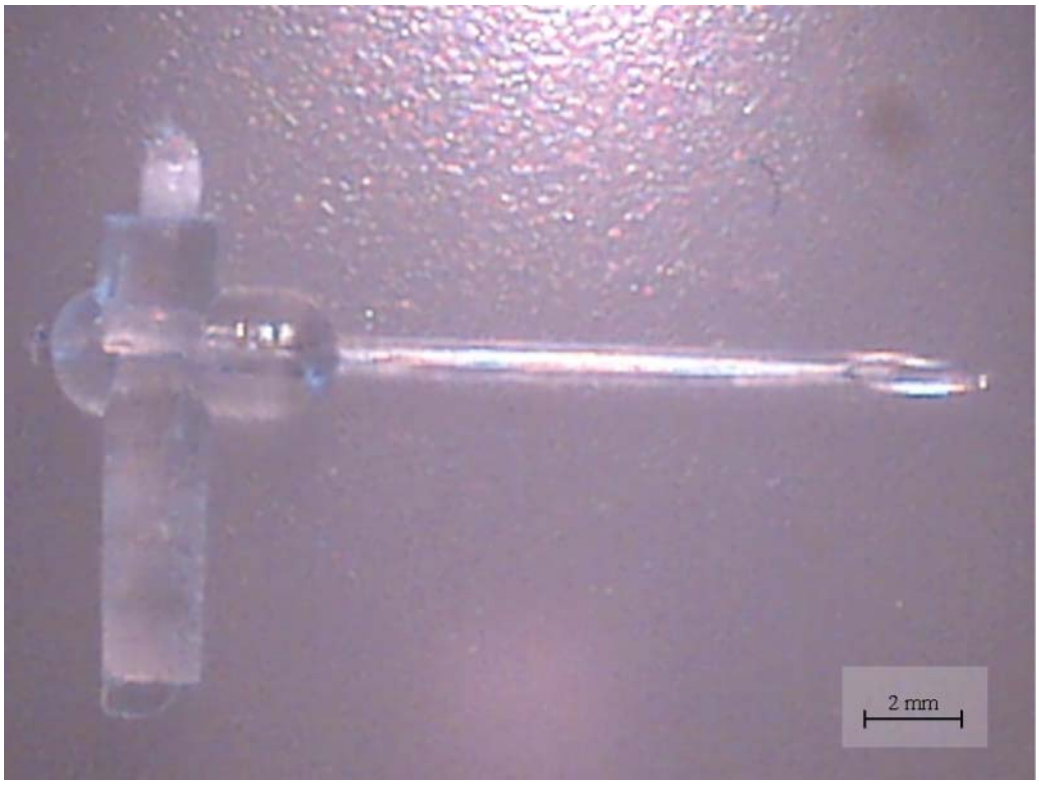

Fig 3.19: Polystyrene Cannula with tip

3.3 SUMMARY

Cannulas, the main body of a hypodermic needle, were fabricated from polymers using micro injection molding. Material selection was performed by considering mechanical properties, biocompatibility, and micro structure. Based on the dimensions of a 22 gage needle, a mold insert for half-inch long cannulas was designed. Two designs to mount the core were devised: V-block and Guide tube. The guide tube design was selected, because it can align more accurately and is simpler. A harness block was designed with a bottle neck shape to keep the core mechanism aligned during injection molding.

Mold inserts and cores were fabricated using SL and conventional machining. Mold insert cores made by SL rapid tooling technique could not endure high temperatures and the ramming impact of the injection nozzle. Hence, metal mold inserts and steel wire cores were used to make cannulas. These metal molds were made using conventional machining and a WEDM (Wire Electro-Discharge Machining). WEDM was used to make grooves that are too small and then were finished by conventional machining to the correct size. For the core alignment mechanism, tubes cut from actual 22 gage needles were used. By giving a guide tube a sharp tip, cannulas with sharp tips were made. Finally, using nanocomposite, polystyrene, polycarbonate, and PMMA, many cannulas were made. In the next chapter, the measurement of the mechanical properties of these cannulas will be presented.

CHAPTER 4

MEASUREMENT OF BUCKLING LOAD

4.1 EXPERIMENTAL SET-UP

To characterize the behavior of the cannula under axial stress, the measurement of the buckling force versus displacement is required. The measurement of force and displacement while pressing the cannula against a rigid plate or skin imitation reveals the mechanical strength of the cannula. This chapter presents the test setup for the cannula samples, the test procedures, and the results.

4.1.1 EXPERIMENT EQUIPMENT

A mechanical testing machine designed solely to measure small forces was chosen to determine the mechanical properties of the cannulas (Model 921A displacement-force test station, Tricor Systems Inc, Elgin, IL) (Fig 4.1). This machine was designed to test membrane switches, conductive rubber, keyboards, and springs. It is suitable for any components for which accurate displacement-force measurements are required. It is equipped with a 40 N (3.6kgf) load cell. Its other specifications are listed in Table 4.1. As the buckling force calculated in Chapter 2 is around 10N, this equipment will be appropriate.

For comparison, a metal cannula from an actual hypodermic needle, whose tip was removed, was also tested. As can be estimated from Young's modulus, a steel cannula is stiffer than a plastic cannula by 50 times. This exceeds the ultimate load of the load cell of the model 921A. Hence, a steel cannula is tested in the mechanical multi-testing station (Model #4466, Instron, Canton, MA) with a 10kN load cell. Fig 4.2 shows that machine in a 3 point bending test configuration. The data acquired from the load cell are saved in ASCII text format and processed by the Excel program.

Table 4.1: Specifications of model 921A displacement-force test station

Range	0 to 3.60 kg (0 to 127 oz)
Resolution	1 g (0.035 oz)
Abs Accuracy	±0.25% of full scale max
Repeatability	±0.1% of full scale max

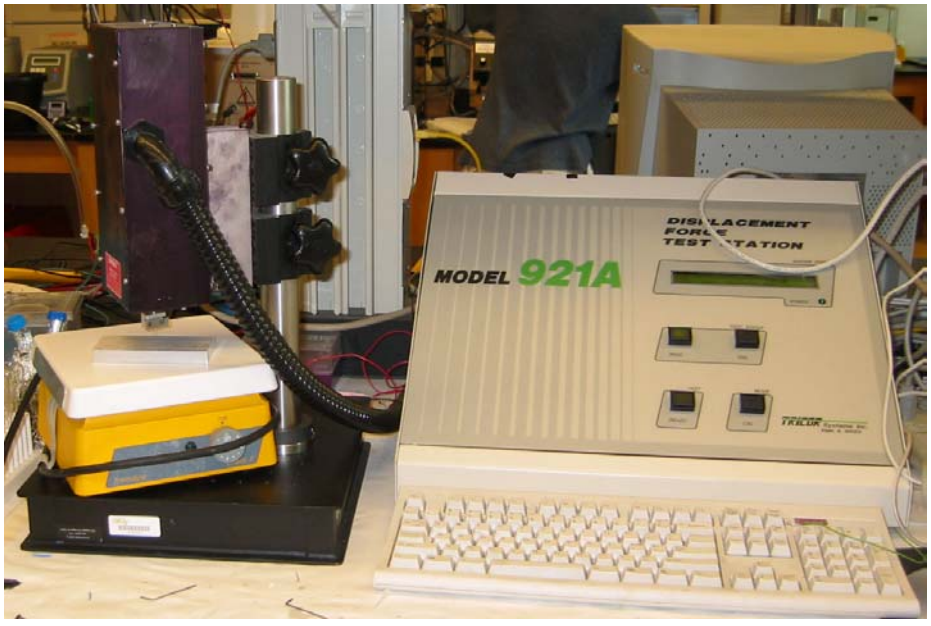

Fig 4.1: Model 921A displacement-force test station (Tricor systems Inc, Elgin, IL)

Fig 4.2: Model 4466 mechanical multi testing station (Instron, Canton, MA)

4.1.2 HOLDER DESIGN

To measure the mechanical properties of cannulas using a mechanical testing machine, a mounting assembly is required. The testing machine can accept a cylindrical shape smaller than 1/8 inch in diameter only. However, a cannula does not have that shape. Hence, an adapting structure which can hold the cannula and be mounted on the machine is needed. The requirements for this holder are accurate alignment and perpendicularity. Plastic cannulas are very weak and easily bent. If an eccentricity or a

non-coaxial loading were applied, then the cannula would buckle in an undesirable mode at a very low load.

Fig 4.3 shows the cannula holder. A cannula is placed in the groove and aligned perpendicular to the index plane (which is parallel to target plate). After alignment, it is locked by the locking plate using two bolts as shown in the Fig 4.4. This assembly is mounted in the testing machine.

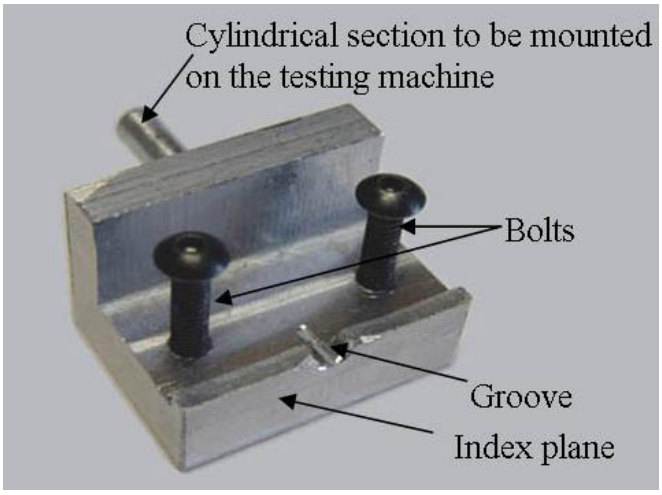

Fig 4.3: A holder for a polymer cannula

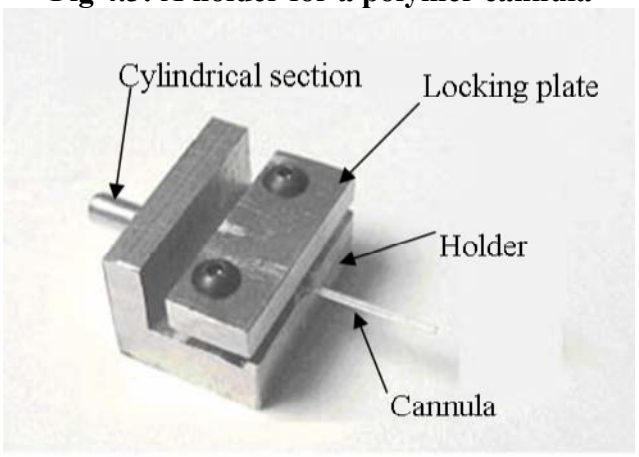

Fig 4.4: A cannula mounted in the adapter

For the testing of metal cannulas, another fixture suitable to the Instron testing machine is designed (Fig 4.5). This fixture is designed to be mounted on the movable head in the 3 point bending test apparatus. Fig 4.8 shows testing fixture mounted on the test machine.

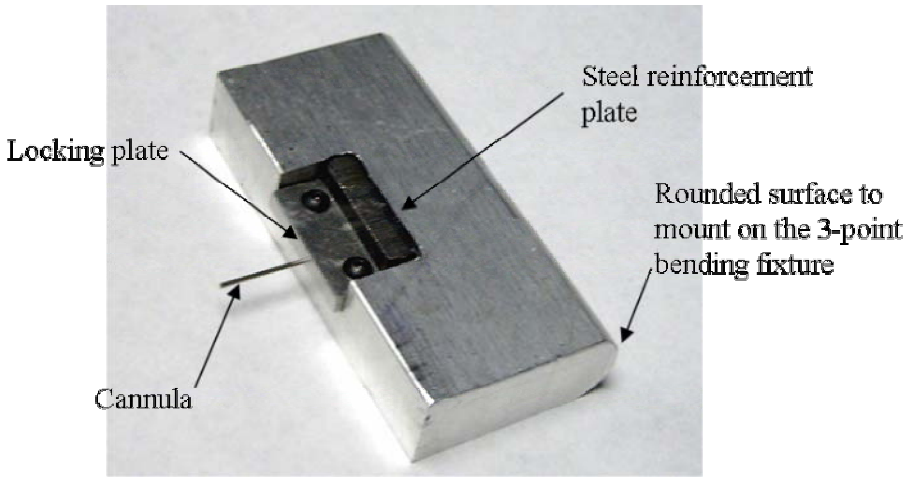

Fig 4.5: Testing fixture for a metal cannula

4.1.3 POKING TARGET

The poking target is a rigid plate which has no or negligibly small deformation when a cannula is poked against it. In this thesis, a 0.25 inch thick aluminum plate is used as the poking target for the plastic cannulas. A hard steel plate is used for the steel cannulas due to its hardness. The test machine drives the cannula towards the stationary target. Though the cannula is aligned perpendicular to the target surface, a slight bend of the cannula due to ejection or a non-perpendicular tip surface can initiate sliding of the cannula on the poking target. This sliding causes the cannula to bend before an axial stress would induce buckling, because the flexural stiffness of the plastic cannula is very

small. To prevent sliding of the cannula, the target plate was machined with a small dent to constrain the tip (Fig 4.6). However, some actual tests showed that it could prevent sliding but could not prevent rotation of tip surface. In other words, buckling occurred in a fixed-pinned condition, not in a fixed-fixed condition (Fig 4.7).

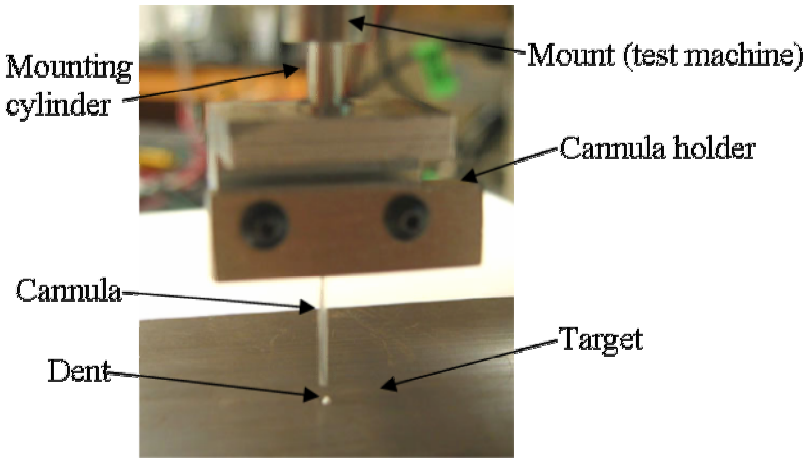

Fig 4.6: A close-up of testing set-up (with rotation permitting target)

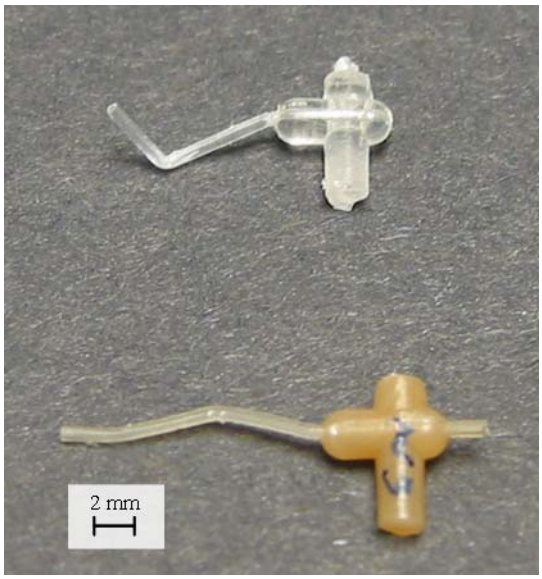

Fig 4.7: Buckling shape (upper) fixed-pinned buckling (lower) fixed-fixed buckling

Finally, to ensure the buckling condition is fixed-fixed, a target plate is cut into small pieces and machined to have a small pit in which to fix the cannula. This small pit holds the end of cannula and prevents it from sliding and rotating. The depth of the trench is 2 ㎜, in other words, some length of the cannula is sacrificed. This small target piece is attached to the cannula with glue. This cannula-target assembly is mounted on the holder and then on the testing machine.

For the test of metal cannulas, a hard steel plate was used. Because the main objective of the buckling tests of the steel cannulas is to get data to compare with the results of plastic needles, a hard steel flat plate was used as the target for this test. Because of rough surface finish, there was enough friction to keep the end of cannula in position. But this configuration could not guarantee it would keep the end of cannula from rotating because the hard target plate deforms too little to surround the tip. Compensation by multiplying by two to convert it into fixed-fixed condition in the calculations is needed. Fig 4.8 shows the testing configuration for buckling of the metal cannula against the hard steel target plate.

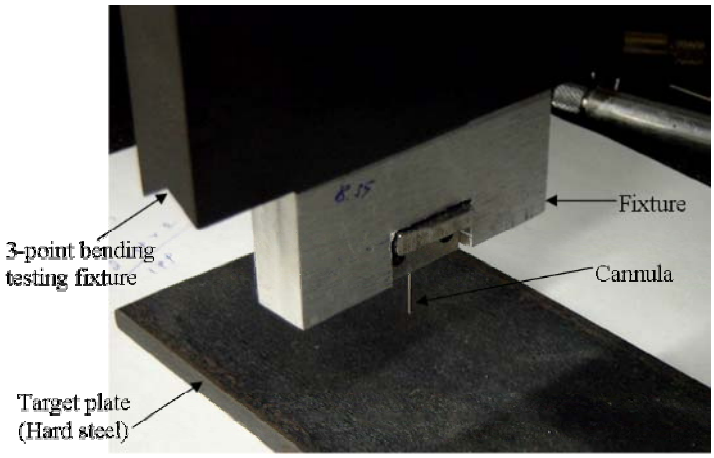

Fig 4.8: Buckling test configuration for a metal cannula

4.2 EXPERIMENTAL OBJECTIVES

The objectives of the buckling measurement experiments are to verify the theoretical buckling load using actual measurement and the analytical (proportional) relationship among the parameters.

The major experimental parameters are the true length (L) of the cannula (=length – depth of trench) and its material's modulus (E). The analytical relationship between L, E, and P_{CR} is shown in Chapter 2: the critical buckling stress is proportional to $1/L^2$ and the Young's modulus of the material (Eq 4.1). This relationship is validated by experiments.

$$P_{CR}\,(Buckling\ Stress) \propto \frac{1}{L^2} \propto E \tag{4.1}$$

In addition to these parameters, the buckling stress also depends on the target condition. If the target permits rotation of the tip, the buckling stress will be half of that of a fixed-fixed condition.

4.3 TESTING PRECEDURES

The algorithm of the test machine is not directly suited to the objective of this test. The testing machine drives a sample against the target until the force reaches the programmed maximum force. Though a sample cannula reaches buckling, the machine does not automatically terminate the test upon buckling because of the low loads at buckling. Hence the machine pushes the cannula into target until the maximum force preset. After reaching the preset, the machine returns to its initial position. This results in

the undesired breakage of the cannula. Also, the data acquisition algorithm tends to ignore forces detected before a very stiff gradient of force is detected. In other words, if a cannula breaks during testing and the mounting holder touches the target, the machine only records the forces measured during the contact between the mounting holder and the target, in other words the stress during the breakage of the cannula. Hence the maximum force preset should be carefully estimated from the results of the analytical and numeric analyses so as not to exceed the ultimate stress of the cannula. In this research, the maximum force preset begins at 2 N and is increased by 1 N at each test. As it approaches the calculated value, it is increased by 0.5 N.

Even with this effort, many cannula samples were broken during testing without noteworthy data. During this research, 30-40 cannulas (including cannulas with tips, the results of which cannot be used here) were made from each material. Ten nanocomposite cannulas, ten polystyrene cannulas, and seven PMMA cannulas were tested. Due to its quality problem and problems with the machine, only the data for four nanocomposite cannulas and three sets of data for three PS and PMMA cannulas were available for further consideration.

After the axial force reaches the critical stress, buckling can occur at any time due to a small perturbation. When buckling occurs, several changes in force and displacement measurement happen. The cannula is bent like an arch. At the same time, the force decreases significantly, because the axial force is relieved by the lateral bending of the cannula. Also the slope of the displacement changes from a steady slope resulting from elastic deformation to a steep slope resulting from buckling. However, for a fixed-fixed condition, the change in strain is negligible, because the deflection of the cannula in the

lateral direction is smaller than that for a fixed-pinned condition. The buckling force is the maximum force measured just before the slope changes. For example, Fig 4.9 and Fig 4.10 show experimental measurements of PMMA cannulas (rotation allowed). In these graphs, one can see that buckling happens at point #50 and the force is 4.56 N.

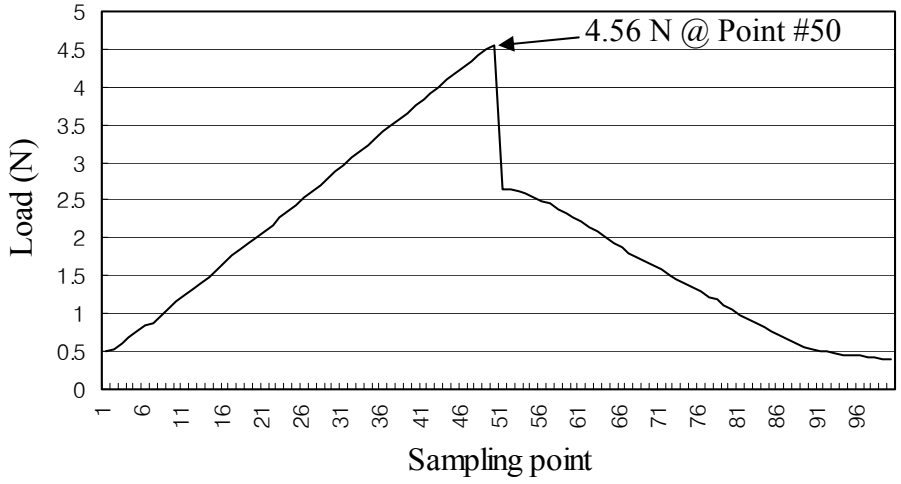

Fig 4.9: Load measurement plot

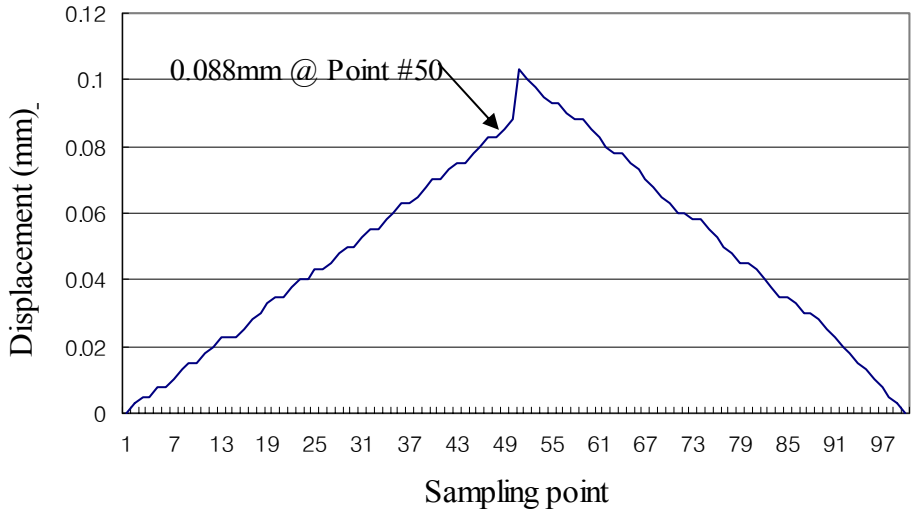

Fig 4.10: Displacement measurement

4.4 BUCKLING LOAD MEASUREMENT

The force and displacement of cannulas under axial loads are measured to characterize the behavior of the cannulas. As mentioned in Chapter 4, a significant change in force or displacement occurs when buckling occurs. However, there is uncertainty in the measurement of the buckling load. The definition of bucking - the buckling critical load at which the state of equilibrium changes to unstable ones - does not mean that buckling occurs. Buckling cannot happen without a small perturbation.

As shown at the end of Chapter 4, the critical buckling load is defined as the load where a significant change in the slope of the load plot takes places (i.e., the point right before the peak). Therefore, there can be difference between the buckling load measured by the method mentioned in Chapter 4 and the critical load at which equilibrium becomes unstable as described in Chapter 2.

4.4.1 BUCKLING OF METAL CANNULAS

The results of the buckling tests of metal cannulas are summarized in Table 4.2. Load plots of these experiments are shown in Fig 4.12 and Fig 4.13. Two cannula samples made from the same lot of hypodermic needles with different lengths were tested. The lengths of the metal cannula samples were 13.55 mm and 14.05mm. It is expected and seen that the small difference in length makes a negligible difference in the buckling load. However, a slight difference in the buckling load resulted (approximately 5%).

After buckling, testing was terminated manually. The samples were bent permanently (Fig 4.11). The bending points were not at the middle. This means the

buckling occurred in a fixed-pinned condition. If buckling occurs in a fixed-fixed condition, the bend will be in the middle of the effective needle length and bent shape should be symmetric, because the loading condition at both ends is identical.

Table 4.2: Results of buckling tests

Sample #	1	2
Length (mm)	13.55	14.05
Buckling load (N)	168.9	160.8

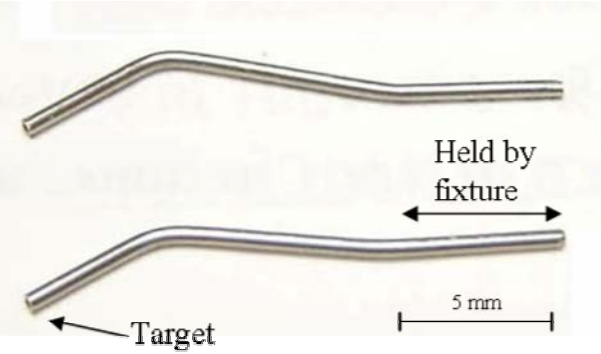

Fig 4.11: Bent cannula samples

Force measurement plots are shown in Fig 4.12 and Fig 4.13. For the longer sample (L= 14.05mm), a small vertical shift can be seen in the displacement. This is due to the vertical slide of cannula being in the locking plate at initial loading. However it did not make a significant difference in the value of the buckling load, as the sliding was finally restrained by the steel backing plate of the holder.

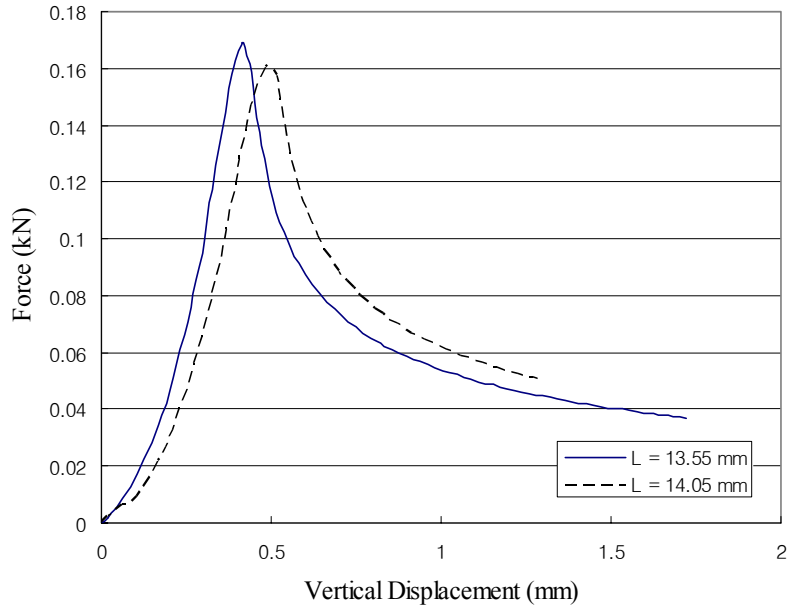

Fig 4.12: Buckling Force of metal cannula

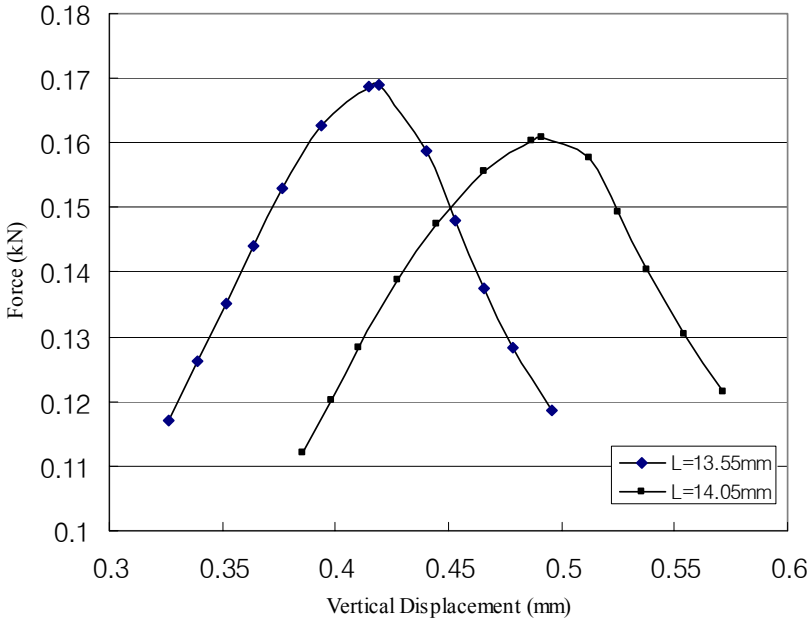

Fig 4.13: Detail of the peaks from Fig 4.14

4.4.2 BUCKLING OF PLASTIC CANNULAS

Cannula samples of three different polymer materials were tested: nylon-based nanocomposite, polystyrene, PMMA. Due to the way that the machine operates, the machine returned automatically after reaching the load preset. Therefore, the load graphs were different from those of the metal ones. After buckling, the cannulas were bent. Fig 4.15 shows the bent shape of a nanocomposite cannula sample. The bending point was located at the middle of the cannula. This bent shape showed that the buckling occurs with same condition at both ends, in other words, a fixed-fixed condition. Thus $4*\pi^2(39.47)$ was used for k [9]. As with the buckling of metal cannulas (Eq 4.1), all the parameters were fixed and exact, therefore, calculated E (modulus) contained all of the experimental errors such as eccentric loading. Hence this E only can be used to compare to the other Es calculated from the buckling measurement of other materials. Further consideration of the errors will be presented later. Fig 4.16 is an axial load plot of the nanocomposite cannulas. Samples 3 and 4 were tested at a faster speed, which makes buckling occur earlier. The buckling forces measured for the nanocomposite samples are summarized in Table 4.3.

$$P_{CR} = k\frac{EI}{L^2} \tag{4.1}$$

Table 4.3: Buckling loads of Nanocomposite cannula

Sample #	1	2	3	4
Length (mm)	10.2	9.4	11.0	12.0
Buckling load (N)	4.47	4.98	4.04	3.55

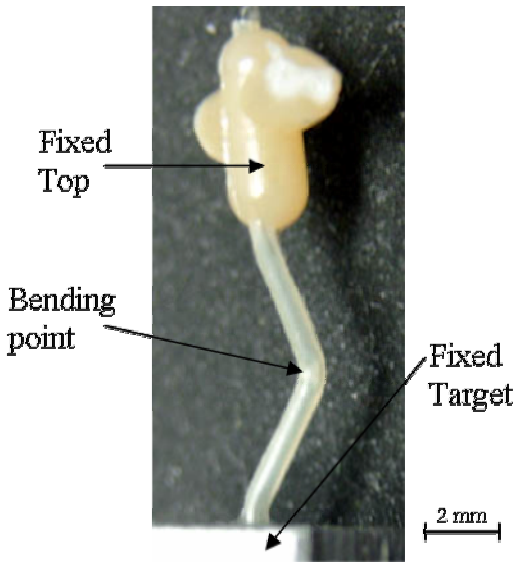

Fig 4.15: Bent shape of Polymer cannula (Nanocomposite)

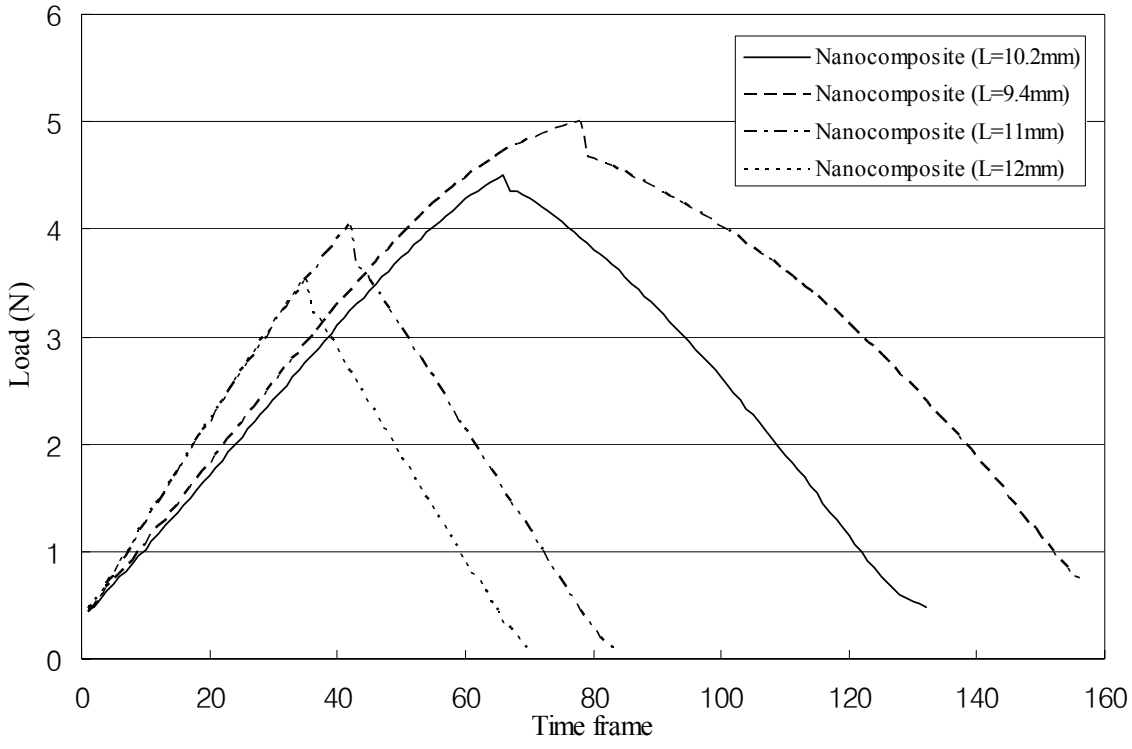

Fig 4.16: Buckling load of nano-composite cannulas

The results of the buckling tests of PMMA are summarized in Table 4.4. The load plots are shown in Fig 4.17. After the buckling, samples fractured because of their brittleness. Because the speed of the cross-head was different, the x-axis (time) had a different scale.

Table 4.4: Test results of PMMA cannulas

Sample #	1	2	3
Length (mm)	9.2	11.3	10.8
Buckling load (N)	9.67	6.52	7.09

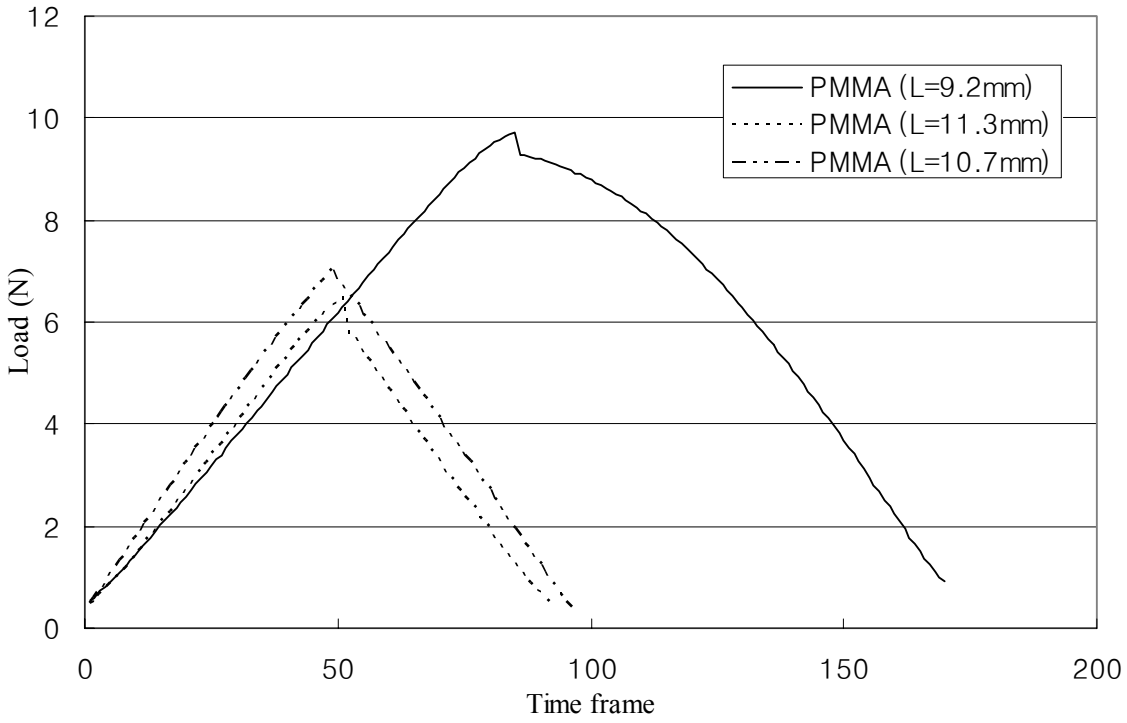

Fig 4.17: Buckling of PMMA cannulas

The results of the buckling tests of PS samples are summarized in Table 4.5. Load plots for each sample are shown in Fig 4.17. After buckling they broke and shattered because of their brittleness.

Table 4.5: Test results of PS cannulas

Sample #	1	2	3
Length (mm)	9.6	10.2	9.5
Buckling load (N)	8.97	8.03	10.02

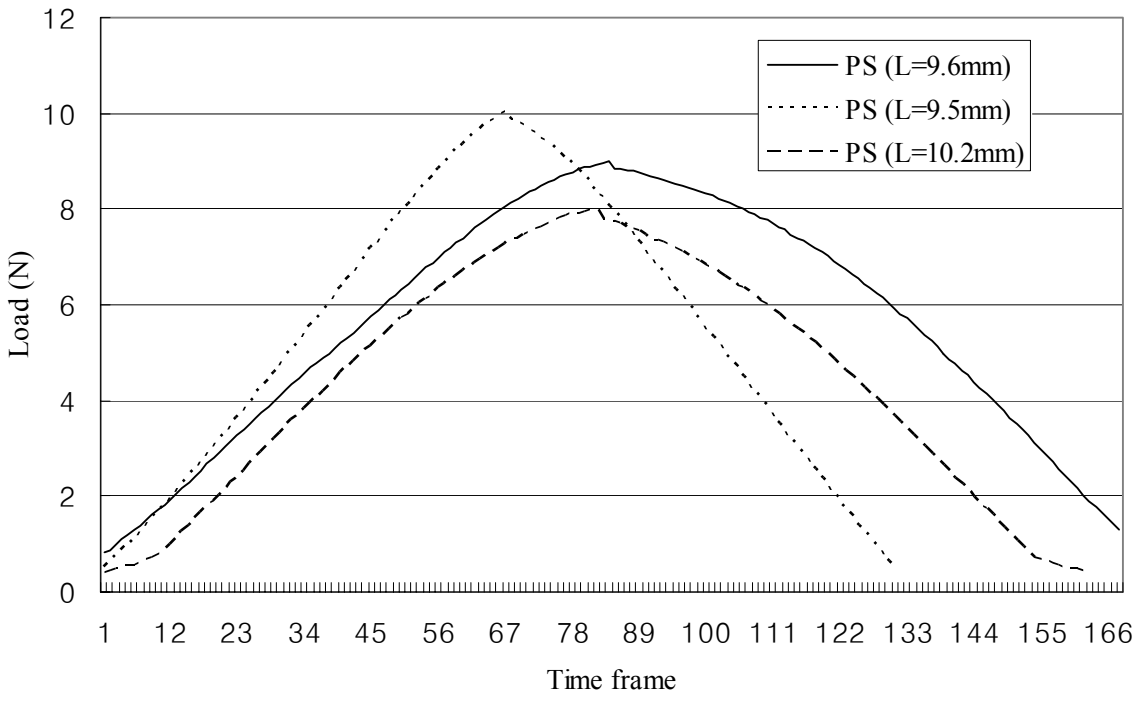

Fig 4.18: Buckling of PS cannulas

4.5 SUMMARY

Cannulas of various materials are tested. Ordinary metal cannulas from real hypodermic needles and the polymer cannulas presented in Chapter 3 are tested. To test each cannula, fixtures and targets are designed to fix them into the testing apparatus.

The buckling stress of a cannula is measured by tracking force and displacement while poking it against a target. The test machine for polymer cannulas ignores the stresses measured when a cannula is broken due to its small value and the machine's buffer size. Hence, the maximum load preset is estimated carefully from the analytical solutions. The buckling moment is determined by the change in slope of the time versus stress curve (usually the maximum load).

However the polymer cannulas broke too easily at comparatively smaller loads than expected. Therefore, only small amounts of data are available for further analyses. In the next chapter, these data will be compared to the results of analytical and numerical analyses. The discrepancy between analytical data and experimental ones will also be discussed.

CHAPTER 5

RESULTS AND DISSCUSSION

The goals of this research were to explore the fabrication of plastic cannulas and to verify their calculated buckling loads. In this chapter, the buckling loads of the plastic and metal cannulas measured in Chapter 4 are compared to the results of the theoretical analyses. Furthermore, discussion of the discrepancy of the values obtained from measurements and analytical analyses will be presented.

5.1 COMPARISON OF THE EXPERIMENTAL DATA WITH ANALYTICAL/NUMERICAL RESULTS TRENDS

In this section, the data measured are used to determine if the buckling load agrees with the theoretical buckling load and the analytical relationship presented in Chapter 2. As presented in the summary of Chapter 2, the analytic and FEA results show very little difference for both loading conditions, fixed-fixed and pinned-fixed.

From Eq 2.2, one can obtain Eq 5.1,

$$P_{CR} L^2 = kEI \tag{5.1}$$

The kEI term represents the properties of the sample and its loading condition. This value should be consistent among the samples if they are made of same material, because the parts have the same dimensions and are tested using the same conditions.

For metal cannulas, these calculations are summarized in Table 5.1. The data for the metal cannulas show only a 2.35% difference in $P_{CR}*L^2$. Therefore, these data agree well with the results of the analytical analyses. From these data, $P_{CR}*L^2$ can be calculated. For the kEI term, as shown in Fig 4.11, buckling occurs in fixed-pinned mode, and $2.046*\pi^2$ (=20.19)[9] can be used for k. The moment of inertia, I, is calculated from the sample's dimensions (Eq 2.2). Finally, E is calculated from the experimental results. However E inherits all the errors, such as eccentric loading and initial bend, from the measured P_{CR}'s because other values are obtained under the assumptions of ideal (analytical) cases. Therefore E cannot be equal to the Young's modulus of that material exactly but can be used as means to compare theoretical and experimental results.

Table 5.1: Pcr*L^2 and modulus of the metal cannula

Sample #	1	2
$P_{CR}*L^2$ ($N\cdot m^2$)	0.03101	0.03174
	2.35% difference (Avg. 0.031375 $N\cdot m^2$)	
E(GPa)	134.3	
E(GPa) (Manufacturer)	210	

As shown in Fig 4.15, a plastic cannula buckles in a fixed-fixed buckling mode. Thus $4*\pi^2$(=39.47) is used as k [9]. From this and other data in Chapter 4, $P_{CR}*L^2$ and E for each material are calculated and summarized in Table 5.2, Table 5.3, and Table 5.4. Theoretical buckling loads recalculated for each sample length and material are also included. These tables show that the form of relationship in Eq 5.1 is well supported for the polymer samples. However, the E of nanocomposite is calculated to be 1.055GPa,

which is 1/4 of the manufacturer's value. A similar comparison of the E's for the other materials shows that they are just half of the actual value for PS and PMMA. Further comparison and discussion for this behavior will be presented in the next section.

Table 5.2: Buckling of nanocomposite cannula

Sample #	1	2	3	4
Length (mm)	10.2	9.4	11.0	12.0
Buckling load (N)	4.47	4.98	4.04	3.55
$P_{CR}*L^2$ (10^{-4} N·m^2)	4.65	4.40	4.89	5.11
	Avg. 4.76 (Standard Deviation 0.31)			
E(GPa) (from experiments)	1.055			
E(GPa) (Manufacturer)	4.0			
Buckling load (N) (Theoretical)	17.35	20.43	14.92	12.54

Table 5.3: Buckling of PMMA cannulas

Sample #	1	2	3
Length (mm)	9.2	11.3	10.8
Buckling load (N)	9.67	6.52	7.09
$P_{CR}*L^2$ ($*10^{-4}$ N·m^2)	8.19	8.33	8.27
	Avg. 8.26 (Standard Deviation $0.07*10^{-4}$)		
E(GPa) (from experiments)	1.83		
E(GPa) (Manufacturer)	3.1		
Buckling load (N) (Theoretical)	16.35	10.96	12.00

Table 5.4: Buckling of PS cannulas

Sample #	1	2	3
Length (mm)	9.6	10.2	9.5
Buckling load (N)	8.97	8.03	10.02
$P_{CR}*L^2$ ($*10^{-4}$ N·m^2)	8.26	8.35	9.0
	Avg. 8.56 (Standard Deviation $0.43*10^{-4}$)		
E(GPa) (from experiments)	1.90		
Buckling load (N) (Theoretical)	15.18	13.45	15.50
E(GPa) (Manufacturer)	3.1		

As shown in the buckling tables for PS, PMMA, and steel cannula, the measured buckling loads are uniformly around 60% of their theoretical loads. The value of nanocomposite was only 25% of its theoretical buckling load. But the $P_{CR}*L^2$ of each sample showed a very small deviation for the same material. This means the analytical relationship is well supported among materials. In next section, consideration of the discrepancies in the values of the modulus found in the measurement will be presented.

5.2 DISCREPANCY IN MODULUS

Because the data of the experiments agree with the analytical relationship presented in chapter 2, the discrepancy of the elastic modulus E is the main issue to be accounted for. The calculated moduli of the materials are summarized in Table 5.5. Most materials show a ratio between manufacturer's values and the experimental ones of around 1.6 except for the nanocomposite, which is about 3.8.

Table 5.5: Discrepancy of modulus between experiment and datasheet

Material	Steel	Nanocomposite	PMMA	PS
Modulus (GPa) (Manufacturer)	210	4.0	3.1	3.1
Modulus (GPa) (Calculated from Experiments)	134.3	1.06	1.83	1.90
Ratio	1.56	3.79	1.69	1.63

This ratio discrepancy may be due to various reasons. These reasons can combine to have an even greater influence. The influence of each reason will be explored later in this section.

1. Eccentric loading

   The center of the cannula is off-center from the axis of the testing machine. Though the testing fixture is made as precisely as possible, eccentric loading is unavoidable.

2. Oblique insertion or bent cannula

   If the end of the cannula is not parallel to the target, then an undesired bending moment is added. This makes the cannula bend more easily. The cannula could be bent during ejection from the injection molding machine, because it is still hot and the ejector pin is located near the end of the part.

3. Core misalignment

   If core wire is bent or misaligned during injection molding, an eccentric hole in the cannula is made, and the thinner section can buckle more easily and fracture can be initiated there.

4. Inelastic deformation

Cannulas can be deformed via inelastic deformation. This reduces the Young's modulus. If the length of cannula is short, the critical buckling load increases. However, if the length of cannula is too short, the material yields due to compression and moduli decrease, before the load reaches to buckling [18].

However, if the ratios of the moduli from the measured buckling load to the manufacturer's reported moduli for the other materials in Table 5.5 are correct and normal, the modulus of the nanocomposite is abnormal. The exact modulus of nanocomposite should be around 2.45GPa, not 1.06GPa. There is another reason in the 57% of loss in modulus ((2.45-1.0550)/2.45=0.57). The material's moisture sensitivity can explain this phenomenon. The matrix material of the nanocomposite is nylon. It is a hydrophilic material that is sensitive to moisture and can be decomposed by the presence of water during processing. The matrix of the nanocomposite from Honeywell is Capron nylon 6. McCarty, Kevin et al. [17] show a 75 % decrease in the elastic modulus of Capron at 60% relative humidity (Fig 5.1). Assuming that the filler of the composite (i.e., nanoclay) is not affected by moisture, the decrease in modulus found in this work is 43.6 % of that in dry condition, which occurs at 30% relative humidity in Fig 5.1. Unfortunately, during testing and fabrication, appropriate measures against moisture were not taken. The pellets were stored in open air without sealing. Because the samples were stored in room air for two months before testing, they most likely were saturated with

moisture. That could be a reason for this discrepancy in the experiments with nanocomposite parts.

To validate this, nanocomposite tensile samples were made from oven-dried pellets (1 hour at 100℃, i.e., almost the same preparation as for the cannulas' fabrication) and stored for a week in room air. Two kinds of samples were prepared. First, samples were stored in room air, and second, samples were dried in vacuum oven (at 0.5 atm and 100℃) for three hours just before testing to remove all the moisture absorbed during 1-week storage. For each condition, four samples were chosen. Uniaxial tensile tests (ASTM-D638) were performed in the Instron 4466 mechanical testing machine (Fig 4.2) with a 10kN load cell. The average modulus from the samples is summarized in Table 5.6. This shows that the nanocomposite is affected by moisture especially before and during injection molding (from 4000MPa to 2921MPa, 27% decrease). The effect of the moisture on resin after molding (i.e., during storage) is not as significant as before and during injection molding (from 2921MPa to 2814MPa, 3% decrease). This mainly resulted from the fact that the absorption of moisture is only skin-deep. Detailed test results for each tensile sample are provided in Appendix. 3.

However, the area-volume ratios of the cannulas and the tensile samples are different. Cannulas are thin walled structures, which can absorb moisture and be easily saturated. Therefore, the effect of moisture during storage after molding is major problem. From this fact, recalculation based on the measured modulus in the tensile test shows that the modulus decrease in the same as the material exposed to around 22% RH air in Fig 5.1. This recalculation is summarized in Table 5.7.

Table 5.6: Results of the tensile test (ASTM-D638)

	Vacuum dried before testing	None
Modulus (MPa)	2921	2814

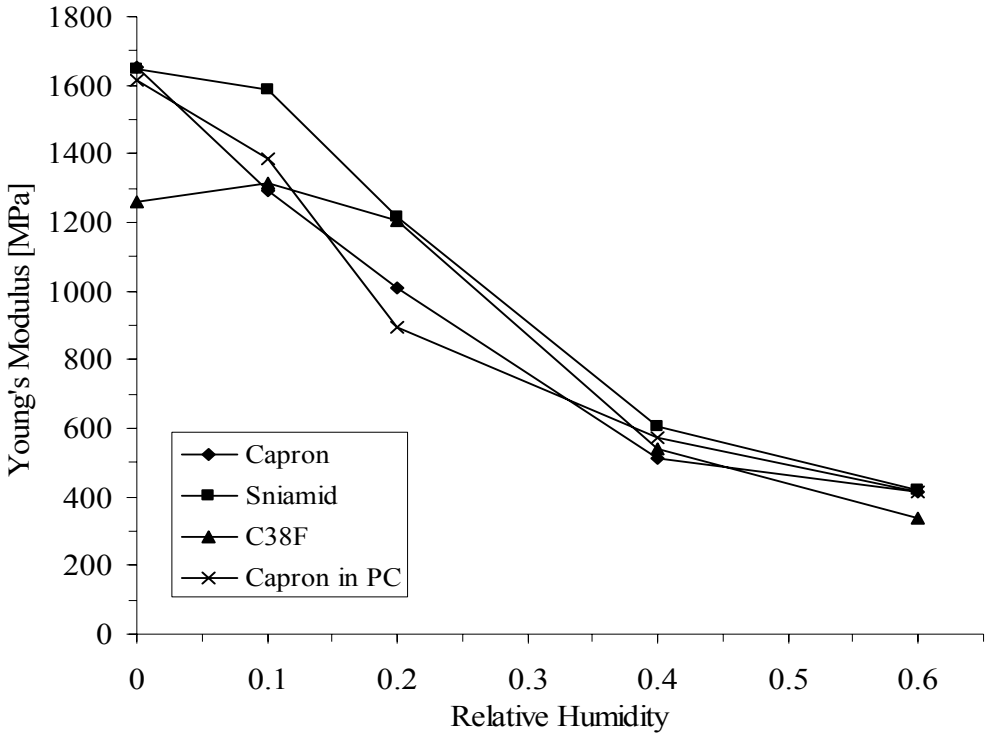

Fig 5.1: Modulus of nylon as a function of relative humidity [17]

Table 5.7: Calculation of modulus loss from moisture

E (measured in tensile test)	2921 MPa	
E (calculated from experimental data of nanocomposite cannula samples)	1055 MPa	
E (Without moisture effect, assuming all the conditions are the same as the other materials.)	1792 MPa	2921/1.63
Loss of modulus due to moisture absorption (%)	41.1	$\frac{1792-1055}{1055}*100$
Corresponding RH (%)	22	From Fig 5.1

To find out how the above-mentioned errors effect on initiation of the buckling at the load lower than the theoretical buckling load, more analyses are required. In next section, analyses to explain these will be presented.

1. Eccentric loading and oblique insertion

In the case of eccentric loading, a bending moment is applied to both ends of the cannula; the eccentricity makes the cannula deflect laterally. But this bending moment does not initiate or contribute to buckling. As can be seen in Fig 5.2, a load-deflection plot, an eccentric loading just makes cannula deflect gradually, not abruptly as pure buckling. Hence the eccentric load does not lower the critical buckling load [19]. Also for the oblique insertion case or the bent cannula case, a bending moment is applied when the target is touched. This is same as the first case, only the bending moment is applied at the end of the cannula.

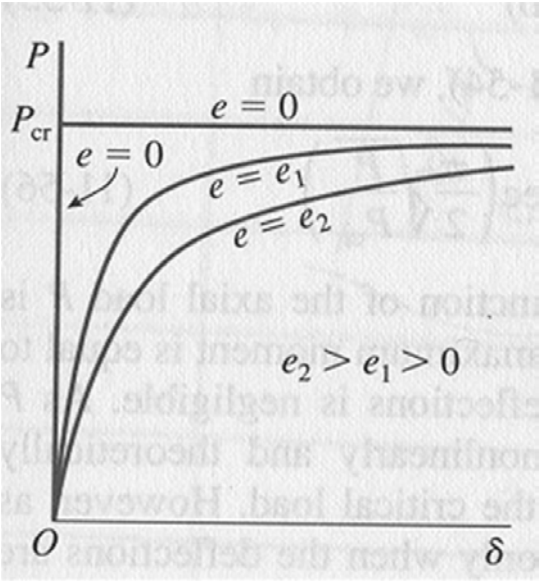

Fig 5.2: Buckling behavior with respect to eccentricity [20]

2. Eccentric loading and oblique insertion

To verify the fourth reason, the eccentric hole in a cannula can initiate buckling at a lower load than theoretically predicted, numerical simulation using FEA is used. Both ends of the core wire are perfectly aligned by a guide during molding of cannula. Therefore eccentric hole is placed in the middle of the cannula. To simplify this analysis, cannulas with simple eccentricities were analyzed.

From the results of finite element analyses using Ansys 7.0 with various eccentricities, the buckling load can be lowered to 80% of the buckling load with a concentric condition. These results are summarized in Table 5.8 and Fig 5.3. The eccentric cannula modeled in Ansys is shown in Fig 5.4.

Table 5.8: Results of analyses for eccentric cannula

Eccentricity (mm)	0	0.01	0.02	0.04	0.06	0.08	0.1	0.12
Relative strength (%)	100	99.9	99.4	97.7	94.8	90.7	85.4	78.9

To apply the result of this analysis to an actual cannula, an equivalent eccentricity is calculated assuming that at its maximum deflection of the core wire barely touches the outer cavity and the slopes are zero at both ends. For this case, the eccentricity is half of the wall thickness (0.075mm), leading to approximately a 9% decrease in modulus.

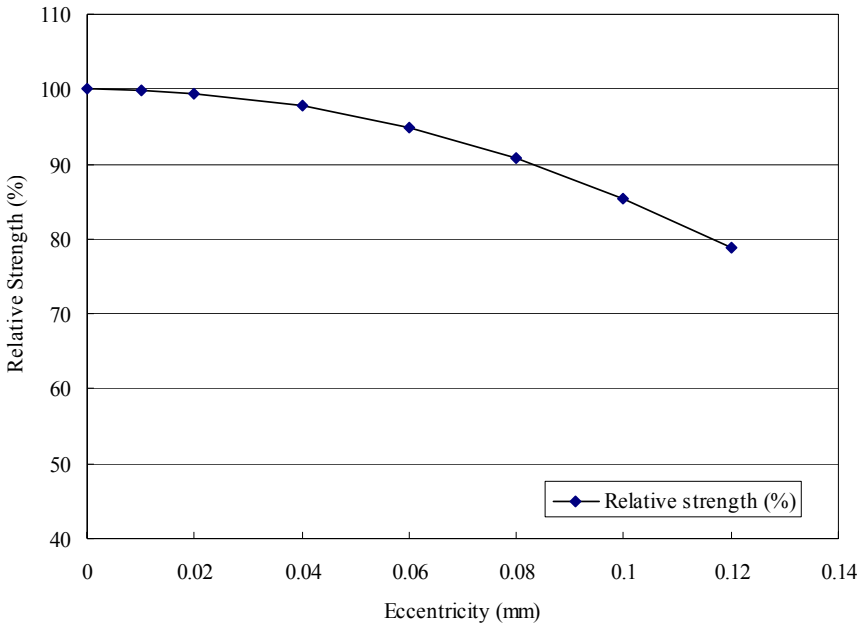

Fig 5.3: Plot of relative buckling strength with respect to eccentricity

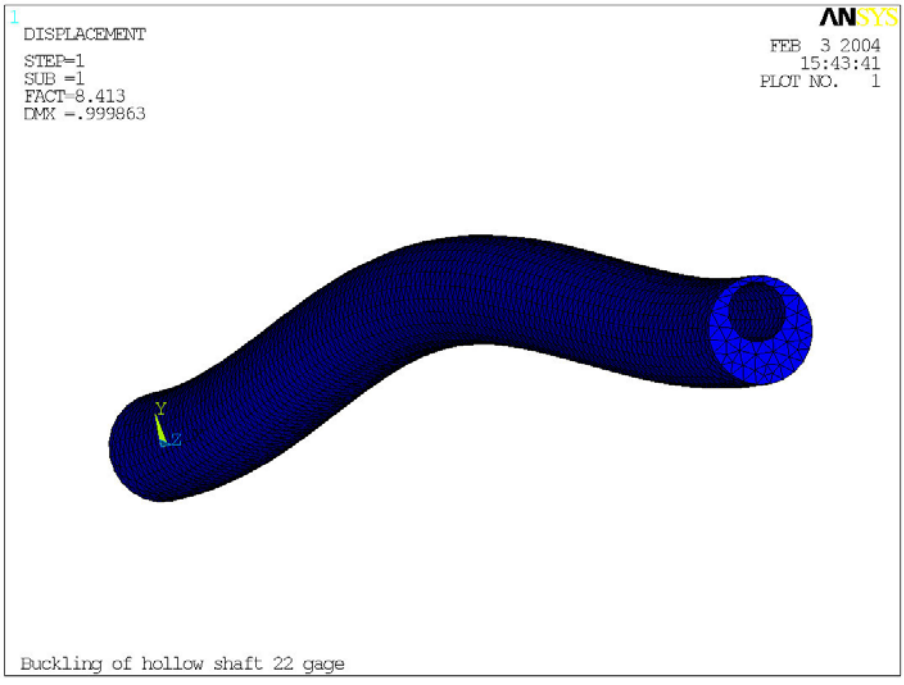

Fig 5.4: Buckling of cannula with eccentric hole (eccentricity = 0.08 mm)

3. Inelastic buckling [21]

The critical load from Euler's approach to elastic buckling is valid only for relatively long columns (cannula). If length of the cannula is intermediate, the stress will reach its proportional limit before buckling begins. After reaching the proportional limit, the material will behave inelastically, in other words, with a reduced modulus. This results in a smaller critical load for buckling. For example, from the buckling of nanocomposite sample in Fig 5.5, the change in the slope of the plot changes means that the modulus changes as the speed of cross-head is constant. This reduction in slope can be seen in many of the plots in Chapter 4.

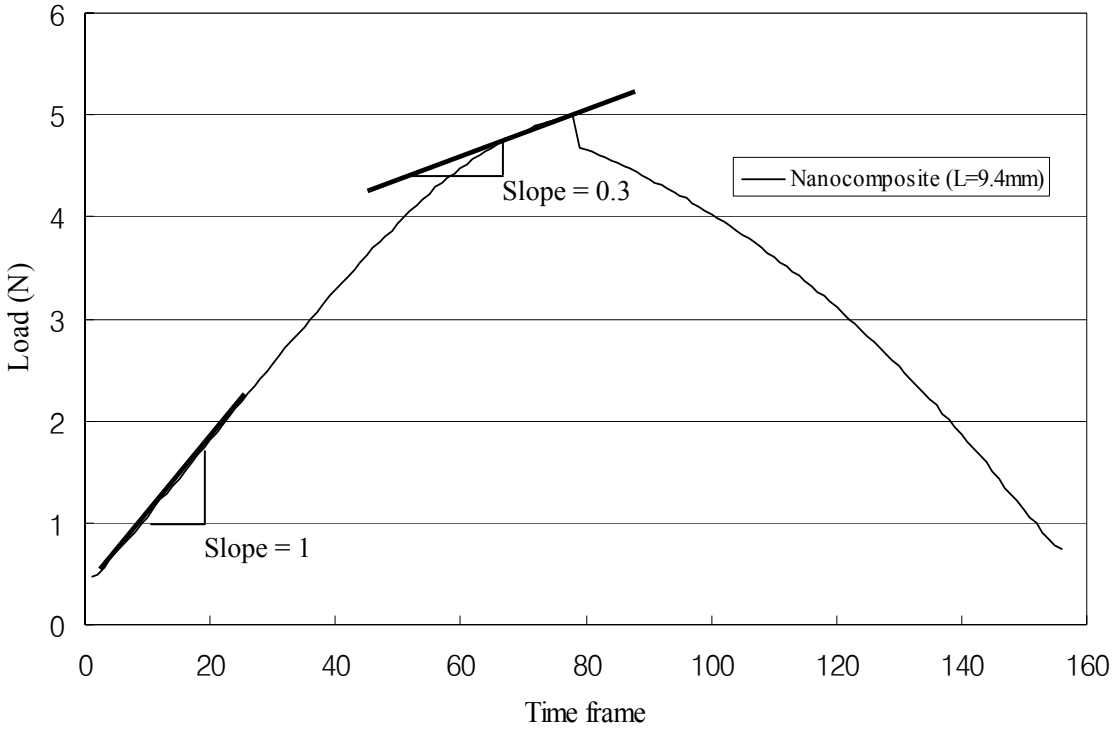

Fig 5.5: Example of inelastic buckling

There are several theories which can calculate reduced modulus and the critical load of this phenomenon, tangent modulus theory, reduced-modulus theory, Shanley theory and Johnson formula [21]. Fig 5.6 shows the difference of the critical load calculated from each method. The Johnson formula is not shown in this plot, because the critical load is not dependent on the lateral deflection but on the length of column.

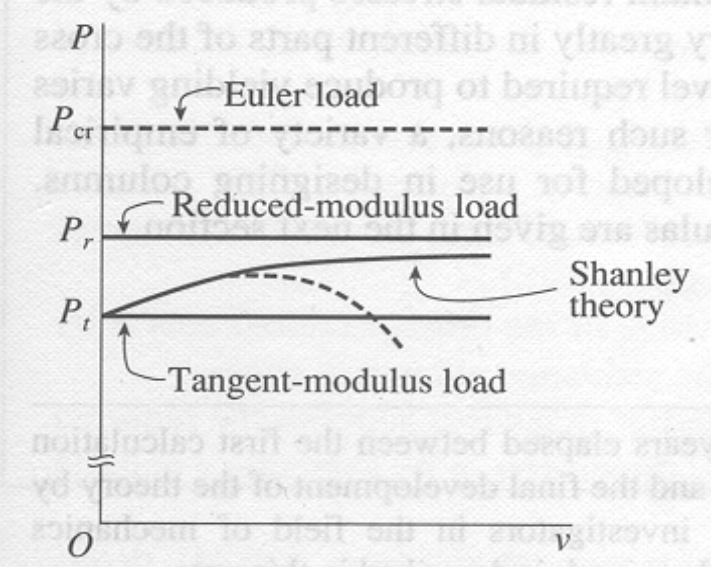

Fig 5.6: Load-deflection diagram for elastic and inelastic buckling [21]

For columns with intermediate length, the parabolic or Johnson formula is more commonly used in engineering field [22]. The general form of this formula is

$$\frac{P_{CR}}{A} = S_Y - b\left(\frac{L}{\kappa}\right)^2 \tag{5.1}$$

where S_Y is the compressive yield stress of the material, A is the cross-sectional area, L is the length of cannula, κ is the radius of gyration of the cross-section ($=(I/A)^{0.5}$) and b is a constant evaluated by fitting a parabola from the Euler curve to the compressive yield stress Fig 5.7. The intersecting point between Euler curve and the parabola is usually

located at $S_Y/2$. From algebra, the corresponding L_{CR} at which two curves meet can be found as (Eq 5.2) and the constant b is found to be (Eq. 5.3). If the length of cannula is shorter than L_{CR}, Euler theory is not fully valid and moduli decrease.

$$L_{CR} = \kappa\pi\sqrt{\frac{8E}{S_Y}} \tag{5.2}$$

$$b = \frac{1}{4E}\left(\frac{S_Y}{2\pi}\right)^2 \tag{5.3}$$

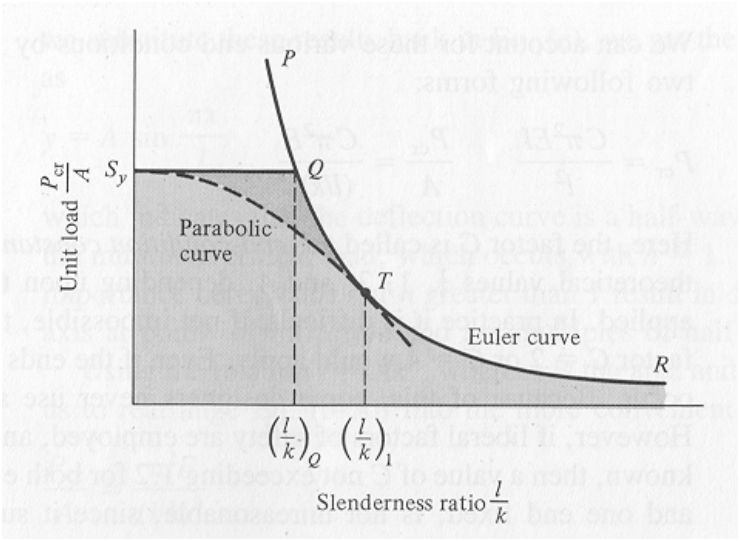

Fig 5.7: Euler curve and parbolic curve

Assuming that the compressive yield stresses of materials are the same as their tensile yield stress, L_{CR} for each material is calculated from data in Chapter 2 and Chapter 3. These L_{CR} are summarized in Table 5.9. As can be seen in the tables, the critical length is longer than the lengths of the cannulas tested in Chapter 4. Thus, the Euler theory is not fully valid for these cannulas. Using the Johnson formula, the critical buckling load of each cannula and the equivalent moduli are recalculated. The results are summarized in Table 5.10, Table 5.11, and Table 5.12.

Table 5.9: Critical length for each material from Eq 5.2

	Steel	PMMA	PS	Nanocomposite
L_{CR} (mm)	49.1	12.0	14.7	15.0

Table 5.10: Summary of the modulus decrease in PS samples

	1	2	3
E (Manufacturer) (MPa)	3100		
Length (mm)	9.5	9.6	10.2
Measured (N)	10.02	8.97	8.03
P_{CR} (Johnson formula) (N)	13.34	13.21	12.41
E (from Johnson formula) (N)	2667	2697	2860
E (from measured data) (N)	2004	1832	1851

Table 5.11: Summary of the modulus decrease in PMMA samples

	1	2	3
E (Manufacturer)(MPa)	3100		
Length (mm)	9.2	10.8	11.3
Measured (N)	9.67	7.09	6.52
P_{CR} (Johnson formula) (N)	10.42	9.46	9.13
E (from Johnson formula) (N)	1954	2444	2582
E (from measured data) (N)	1813	1832	1845

Table 5.12: Summary of the modulus decrease in Nanocomposite samples

	1	2	3	4
E (MPa) (Measured in Tensile test)	2921			
Length (mm)	9.4	10.2	11	12
Measured (N)	4.98	4.47	4.04	3.55
P_{CR} (Johnson formula) (N)	9.18	8.80	8.38	7.82
E (from Johnson formula) (N)	1797	2027	2247	2496
E (from measured data) (N)	975	1030	1083	1133

As can be seen in the tables, the moduli from Johnson's formula show smaller errors. This means that Johnson's formula can predict the buckling of these cannulas better than Euler theory. This shows that the inelastic deformation of the materials is big reason for the discrepancy in moduli. Though it is not suitable for the longer cannulas

which will be made in future, Johnson's formula is more suitable for the short cannula used in this thesis.

5.3 SUMMARY

Using the data measured in Chapter 4, the analytical analyses and experimental results were compared. The experimental results agree well with the analytical relationship, P_{CR} is proportional to $1/L^2$. But a comparison of the calculated modulus to the manufacturer's modulus shows a 1.63 times (on average) smaller modulus is obtained from experimental data. This phenomenon may result from unexpected bending moments due to eccentricity in loading, cannula samples bent during fabrication, oblique insertion, and cannulas with eccentric or uneven wall-thickness from bent core wires during injection molding. Euler buckling theory is not fully valid for the length of the cannula used in this thesis because an inelastic deformation occurs (i.e., the modulus reduces during the compression) during compression in short cannula. Johnson's column formula is hence a better predictor of buckling.

An even bigger difference is calculated for the nanocomposite samples. This discrepancy is due to the matrix of composite, nylon. As it is hydrophilic, the modulus can be decreased severely by the absorption of moisture from room air.

CHAPTER 6

CONCLUSIONS AND RECOMMENDATIONS

In this chapter, the conclusions of the research and the recommendations for future work are presented. The results of analyses using analytical and numerical methods and the experimental data are related to the original objectives set in Chapter 1. In addition to this, the limitations and shortcomings of the research are discussed, and some more topics to be improved upon are stated in the recommendations for future work.

6.1 CONCLUSIONS

The hypodermic needle is the one of most common tools in the medical field. The cannula is one of the main parts of a hypodermic needle. Its functional requirements are hollowness to transfer liquid (drugs, blood, etc) and structural stiffness to transfer the force needed to penetrate skin from a syringe to the tip. This research covered structural analyses of and experiments with cannulas. Buckling failure, which is the most likely failure mode in the cannula, was focused on.

6.1.1 ANALYSES

Buckling may be a major form of failure for plastic cannulas, as a cannula may break after buckling. During buckling, an axial load is changed into a bending moment

due to eccentric loading. The most critical moment in the buckling of a cannula is just before penetration into skin. At that moment, the axial load applied to cannula is the largest and the effective length of cannula is the longest.

Analytic calculation yielded $P_{CR} = kEI/L^2$, where k is a load condition dependant constant. From a half-inch (12.7mm), 22 gage cannula model, 11.19 N was calculated as P_{CR} for nanocomposite cannula with both ends fixed.

To get more accurate results and to accommodate more complex analyses (i.e. cannula with a beveled tip and a piercing situation), numerical analyses using finite element method were also tried. From the stiffness matrix of the cannula structure obtained from simple axial loading situation with unit load, singularities (eigenvalues) were found using Lanczos's method algorithm. Ansys outputs the mode shape and its critical load as a form of load factor (multiplier) of initially given load.

A 22 gage cannula model (L=12.7mm) was meshed using various mesh sizes (0.15mm, 0.12mm, 0.09mm) to verify convergence. Both fixed-pinned and fixed-fixed conditions are analyzed. From these Finite Element Analyses, results with small variability (less than 5%) can be found. Also, a skin model is introduced to simulate the situations when a cannula is poking against skin. From these analyses boundary, condition at the interface between cannula and skin is determined to be a fixed-fixed condition.

6.1.2 FABRICATION

Plastic cannulas are made using a microinjection molding technique. Molds made of rapid tooling material and of conventional steel are used. Though the rapid tooling

materials took much less time to make and showed good accuracy, they showed weaknesses during injection molding, such as melting problem at high temperature. So, steel molds were used. Cannulas are hollow structures and need cores during molding to make them hollow. Straightened steel wire was used as a core. Using four different materials: PS, PMMA, nylon-based-nanocomposite and PC, 22 gage cannulas were fabricated. Among those cannulas, PS, PMMA, and nanocomposite cannulas were tested experimentally.

6.1.3 EXPERIMENTS

Whether buckling occurs or not can be determined by a bent shape like an arch and an abrupt change of slope in the force-displacement plot, because buckling relieves the axial load by changing it into a bending moment. The experimental data followed the trends of Euler's buckling theory; P_{CR} is proportional to $1/L^2$. E can be calculated from the experimental P_{CR} and dimensional data. However, these moduli are around 60% of the manufacturer's values and even 1/4 for the nylon 6-based nanocomposite.

Several explanations can be found for these experimental data. The first is an unexpected bending moment resulting from an eccentric loading due to off-centered installation on the cross-head of the machine or to oblique insertion. An initially bent cannula during ejection from the mold can add an unexpected bending moment. The quality control of cannulas can be another reason. Bent or misaligned core wires produce eccentric cannulas, and the thinner wall sections can buckle or initiate fracture more easily. The last reason is that Euler buckling theory is not fully valid for the length of the

cannula used because inelastic deformation occurred (i.e., the modulus is reduced) during compression. Using Johnson's column formula, buckling can be better predicted.

For the nylon 6 based nanocomposite cannulas, there is another reason - the moisture issue. Cannulas were saturated with moisture during storage in room air. This weakens the cannulas. McCarty et al. found that nylon 6 shows up to a 60% decrease in modulus in 60% RH.[17].

6.1.4 GUIDELINE FOR TIP DESIGN

Cannulas made of polymer materials showed the ability to withstand an axial load. From analyses and experiments, in most cases, cannulas endured 60% of the limit of theoretical model. If tip is designed and made with very small tip area, less force will be required to penetrate skin. For example, a tip with a 10000 μm^2 area (0.1mm * 0.1mm) needs 1.2 N to penetrate the skin [15])**,** because the insertion force is proportional to sharpness (surface area) of the tip. The shape of the tip needs to be optimized to avoid structural failure.

6.2 RECOMMENDATIONS FOR FUTURE WORKS

In this research, the mechanical properties and the fabrication of polymer cannulas are investigated. The buckling of cannulas does not tell the complete story of hypodermic needles; the cannulas used in this thesis didn't have tips to penetrate skin. Though some samples were fabricated using the tip of an actual needle as a mold fracture, they were reverse in shape to the needle, and hence was not optimized to penetrate skin with a small

force and little pain. For further research, tips should be integrated and the complete structure should be analyzed. The flow of the molten plastic is very complex: high-viscosity, creeping flow (very low Reynold's number), and two-phase flow. To add a tip successfully, the flow of molten plastic near the tip is another issue to investigate. A sharp tip is not a shape easily made with molten plastic because of its high surface tension. CFD would be a good tool to analyze this microscopic situation.

All the cannulas fabricated in this research are less than 12.7mm because of mold restrictions. However the lengths of the needles actually used for vaccination are usually 20mm to 25.4mm. To fabricate longer needles, two things must be considered. First, the flow of molten polymers in narrow channels should be considered thoroughly. The longer the channel is, the higher is the possibility of short shots and other defects. Second, a mechanism for mounting the core assembly should be enhanced to exert more tension on the core wire. The core is very thin wire and is exposed to the high pressure of molten plastic flow. This wire is easily bent and to prevent this higher tension is required.

APPENDIX 1

DATASHEET OF POLYMER MATERIALS

AEGIS™ XA-2908

Aegis XA-2908 was developed to perform as an extrusion and injection molding resin. The unique characteristics of this resin is its ability to reduce the rate of oxygen transmission in film packaging and rigid packaging structures containing Nylon by 50% while maintaining or improving the flavor and aroma barrier, toughness and clarity. Aegis XA-2908 has been extruded and co-extruded as monolayer and multilayer film structures, it has also been injection molded providing a surface finish very similar to Nylon 6. In both extrusion and injection molding Nylon processing conditions were used producing high quality films and parts. The ease of processing allows vendors to utilize their present molding equipment and technology to broaden their market application of nylon.

TYPICAL PROPERTIES

	DAM	50% RH	ISO Test
PHYSICAL			
Density, g/cm^3	1.13	-	1183
MECHANICAL			
Tensile Modulus, MPa			527
23°C	4000	-	
Tensile Strength, Yield, MPa			527
23°C	92	-	
Tensile Strength, Break, MPa			527
23°C	89	-	
Break Elongation, %			527
23°C	6.3	-	
Flexural Strength, MPa			178
23°C	126	-	
Flexural Modulus, MPa			178
23°C	3,700	-	
IMPACT			
Izod Impact, J/M			180
-40°C	3.7	-	
23°C	4.6	-	
THERMAL			
Melting Point, °C	220	-	3146
Heat Deflection @ 264 psi (1.8 MPa) °C	108	-	75

Table A1.1: Properties of polymer materials used in this work [24]

PROPERTY	ASTM TEST	PS	PC	PMMA
Manufacturer & Name	N/A	Chevron GPPS 3600	GE Lexan 121R-111	Atohaas Plexiglas V Grade
Melt Flow, Condition G	D-1238	13.0 g/10 min	17.5 g/10 min	3.7 g/10 min
Izod Impact Strength	D-256	0.35 ft-lb/in notch	13.0 ft-lb/in notch	0.30 ft-lb/in notch
Vicat Softening Temperature	D-1525	209 ^{o}F (98.3 ^{o}C)	310 ^{o}F (98.3 ^{o}C)	232 ^{o}F (98.3 ^{o}C)
Heat Deflection Temperature	D-648	180 ^{o}F (82.2 ^{o}C)	280 ^{o}F (82.2 ^{o}C)	221 ^{o}F (82.2 ^{o}C)
Tensile Stress	D-638	6800 psi	9000 psi	10200 psi
Tensile Elongation at Rupture	D-638	3.0 %	125.0 %	6.0 %
Tensile Modulus	D-638	4.5 * 10^5 psi	3.4 x * 10^5 psi	4.5 * 10^5 psi
Flexural Strength	D-790B	9000 psi	14000 psi	15000 psi
Flexural Modulus	D-790B	4.5 * 10^5 psi	3.4 * 10^5 psi	45 * 10^5 psi
Specific Gravity	D-792	1.04	1.20	1.19
Suggested Nozzle Temperature	N/A	425 ^{o}F (218.3 ^{o}C)	530-570 ^{o}F (277-299 ^{o}C)	410-482 ^{o}F (210-250 ^{o}C)
Suggested Melt Temperature	N/A	400-415 ^{o}F (204.4-212.8^{o}C)	540-580 ^{o}F (282-304 ^{o}C)	392-446 ^{o}F (200-230 ^{o}C)
Suggested Mold Temperature	N/A	150-170 ^{o}F (65.69-76.7^{o}C)	160-200 ^{o}F (71.1-93 ^{o}C)	160 ^{o}F (71.1 ^{o}C)
Glass Transition Temperature	N/A	194-212 ^{o}F (90-100 ^{o}C)	150 ^{o}F (302 ^{o}C)	194-212 ^{o}F (90-100 ^{o}C)
Consistency Index	N/A	21840	4310	42700
Power Law Index	N/A	0.26	0.67	0.25

APPENDIX 2

SOURCE LIST OF APDL CODE FOR

NUMERICAL ANALYSES

Simple Compression and Buckling

Fixed-fixed condition.

```
/PREP7
/title, Buckling of hollow shaft 22 gage
ANTYPE,STATIC              ! STATIC ANALYSIS
PSTRES,ON
cyl4,0,0,.356,,.197,,12.7
!*
ET,1,SOLID95
!*
MPTEMP,,,,,,,,
MPTEMP,1,0
MPDATA,EX,1,,4000
MPDATA,PRXY,1,,.418

! meshing*
ESIZE,0.09,0,
MSHAPE,1,3D
MSHKEY,0
!*
CM,_Y,VOLU
VSEL, , , ,      1
CM,_Y1,VOLU
CHKMSH,'VOLU'
CMSEL,S,_Y
!*
VMESH,_Y1
!*
CMDELE,_Y
CMDELE,_Y1
CMDELE,_Y2
finish


!*fixed end
/SOLU
FLST,2,1,5,ORDE,1
FITEM,2,1
!*
/GO
```

```
DA,P51X,ALL,0

FLST,2,1,5,ORDE,1
FITEM,2,2
/GO
!*
DA,P51X,UX,0
FLST,2,1,5,ORDE,1
FITEM,2,2
/GO
!*
DA,P51X,UY,0

FLST,2,1,5,ORDE,1
FITEM,2,2
/GO
!*
DA,P51X,UZ,-0.011494


allsel,all
solve
finish

/SOLU
ANTYPE,BUCKLE
BUCOPT,LANB,1
!OUTPR,NSOL,ALL
allsel,all
SOLVE
FINISH

/SOLU
EXPASS, ON
MXPAND,1
OUTPR
OUTRES
allsel,all
SOLVE
save
finish

/POST1
!SET, LIST
SET,,1
PLDISP
```

Fixed-pinned condition.

```
/PREP7
/title, Buckling of hollow shaft 22 gage
ANTYPE,STATIC            ! STATIC ANALYSIS
PSTRES,ON
cyl4,0,0,.356,,.197,,12.7
```

```
!*
ET,1,SOLID95
!*
MPTEMP,,,,,,,,
MPTEMP,1,0
MPDATA,EX,1,,4000
MPDATA,PRXY,1,,.418

! meshing*
ESIZE,0.12,0,
MSHAPE,1,3D
MSHKEY,0
!*
CM,_Y,VOLU
VSEL, , , ,       1
CM,_Y1,VOLU
CHKMSH,'VOLU'
CMSEL,S,_Y
!*
VMESH,_Y1
!*
CMDELE,_Y
CMDELE,_Y1
CMDELE,_Y2
finish


!*fixed end
/SOLU
FLST,2,1,5,ORDE,1
FITEM,2,1
!*
/GO
DA,P51X,ALL,0

FLST,2,1,5,ORDE,1
FITEM,2,2
/GO
!*
SFA,P51X,1,PRES,3.620
FLST,2,1,5,ORDE,1
FITEM,2,2
/GO
!*
DA,P51X,UX,0
FLST,2,1,5,ORDE,1
FITEM,2,2
/GO
!*
DA,P51X,UY,0


allsel,all
solve
finish
```

```
/SOLU
ANTYPE,BUCKLE
BUCOPT,LANB,1
!OUTPR,NSOL,ALL
allsel,all
SOLVE
FINISH

/SOLU
EXPASS, ON
MXPAND,1
OUTPR
OUTRES
allsel,all
SOLVE
save
finish

/POST1
!SET, LIST
SET,,1
PLDISP
```

APPENDIX 3

Materials testing of XA-2908

Table A3.1: Sample preparation for tensile test

Samples	1	2
Injection condition	Dried 1 hour (at 100℃) before molding.	
Preparation	Stored 1 week in room air and dried in vacuum oven (at 100℃, 0.5atm) for 3 hours.	Stored 1 week in room air.
Test method	Tensile test (ASTM-D638). Instron 4466 multi-purpose mechanical testing machine.	

Table A3.2: Tensile test results of Vacuum dried samples

	1	2	3	4	AVG	S.D.
Displacement at peak (mm)	8.375	2.785	9.116	7.654	6.982	2.861
% strain at peak	8.375	2.785	9.116	7.654	6.982	2.861
Load at peak(kN)	3.209	2.407	3.192	3.189	2.999	0.395
Stress at peak (Mpa)	79.961	59.977	79.538	79.463	74.735	9.841
Displacement at Break (mm)	21.575	3.236	17.247	15.233	14.323	7.851
% Strain at Break (%)	42.471	6.370	33.950	29.985	28.194	15.454
Load at Break (kN)	2.264	1.603	2.259	2.181	2.077	0.318
Stress at Break (Mpa)	56.424	39.949	56.291	54.351	51.754	7.927
Load at 0.20% Yield (kN)	1.383	1.650	1.426	1.689	1.537	0.155
Stress at 0.20% Yield (Mpa)	34.463	41.113	35.520	42.076	38.293	3.856
Young's Modulus (MPa)	2869.33	2968.26	2945.05	2904.54	2921.80	43.780
Energy to Break Point (J)	51.875	5.404	41.968	37.110	34.089	20.086
Tensile Energy Absorption (N/mm)	80.406	8.376	65.050	57.520	52.838	31.134

Table A3.3: Tensile test results of non-treated samples

	1	2	3	4	AVG	S.D.
Displacement at peak (mm)	4.967	4.888	5.035	4.888	4.945	0.071
% strain at peak	4.967	4.888	5.035	4.888	4.945	0.071
Load at peak(kN)	3.260	3.208	3.254	3.227	3.237	0.024
Stress at peak (Mpa)	81.942	81.215	82.380	81.696	81.808	0.486
Displacement at Break (mm)	4.947	6.348	16.345	9.714	9.339	5.081
% Strain at Break (%)	9.895	6.348	16.345	19.428	13.004	5.955
Load at Break (kN)	3.260	3.141	1.683	2.028	2.528	0.791
Stress at Break (Mpa)	81.942	79.519	42.608	51.346	63.854	19.836
Load at 0.20% Yield (kN)	1.618	1.750	1.476	1.637	1.620	0.113
Stress at 0.20% Yield (Mpa)	40.676	44.312	37.366	41.444	40.949	2.856
Young's Modulus (MPa)	2840.60	2843.12	2814.30	2810.75	2827.19	17.03
Energy to Break Point (J)	5.218	7.421	20.197	23.334	14.042	9.054
Tensile Energy Absorption (N/mm)	8.290	11.874	32.315	37.334	22.453	14.505

REFERENCES

[1] Miller, M. A. and Pisani, E. The cost of unsafe injections, Bulletin of the World Health Organization, 1999, **77** (10), pg 808.

[2] Angelova, N., Hunkeler D., (1999) Rationalizing the design of polymeric biomaterials, Trends in Biotechnology, Volume 17, Issue 10, Tibtech October 1999 (Vol 17). pp. 411-412.

[3] Park, J. B. and Lakes, R. S. Biomaterials: An introduction. 2nd ed. Plenum Pub Corp, New York, 1992, pp. 147-157

[4] Worley II, D. C., Akkapeddi, M. K. Socci, E. P. Deformation and Orientation of Polyamide 6 Nanocomposite, Technical paper, New Technologies Group, Honeywell Engineering Applications and Solutions, Morristown, NJ 07962 http://www.asplastics.com:80/literature/techpapers/0708.pdf

[5] XA-2908 Datasheet, New Technologies Group, Honeywell Engineering Applications and Solutions, Morristown, NJ 07962

[6] Injection Molding Training School. SYCAP/HIRPO MIII Operation Course. Sumitomo Heavy Industries, LTD. Plastic Machinery Division, Technical Center, Chiba-Ken, Japan, 1988

[7] Medical Murray incorporated, Operator/Maintenance Manual, Sesame™ .080 Nanomolding™ Machine, Buffalo Grove, IL 60089, May 2001.

[8] Gere, J. M., Timoshenko, S. P. Mechanics of Materials, (4th SI edition) Stanley Thornes (Publisher) Ltd, Cheltenham, UK, 1999, pg 737

[9] Gere, J. M., Timoshenko, S. P. Mechanics of Materials, (4th SI edition) Stanley Thornes (Publisher) Ltd, Cheltenham, UK, 1999, pg 755.

[10] Ansys Inc. Online help for Ansys Release 7.0 Theory reference, shape functions of 3D solids.

[11] Ansys Inc. Online help for Ansys Release 7.0 Structural analysis guide, Chapter 7. Buckling analysis, 7.5. Procedure for Eigenvalue Buckling Analysis.

[12] Plastic design library, Fatigue and tribological properties of plastics and elastomers., 1995, pp.325-327

[13] Hendricks, F.M., et al., Mechanical Properties of Different Layers of Human Skin, Dept. of Materials Technology, Eindhoben Univ. of Technology, PO Box 513, 5600 MB Eindhoben, the Netherlands http://www.bmt.tue.nl/pdf/postersonderzoekdag2001/fhendriks.pdf

[14] Oomens, C.W.J., et al., Deformation Analysis of a Supported Buttock Contact, BED- Vol. 50, 2001 Bioengineering Conference. ASME, 2001

[15] Davis, S. P., Hollow Microneedles for molecular transport across skin , Doctorate Thesis, Summer, 2003, Georgia Institute of Technology

[16] McFarland, Andrew W. Production and Analysis of Injection Molded Micro-optics components Master of Science Thesis, Summer, 2003, Georgia Institute of Technology, pg 53

[17] McCarty, K. et al., Glass transition, moisture content and mechanical characteristics of Nylon, Princeton University http://gobo.princeton.edu/reports/Documents/memos/Cristian-NylonTests.pdf

[18] Gere, J. M., Timoshenko, S. P. Mechanics of Materials, (4th SI edition), Stanley Thornes (Publisher) Ltd, Cheltenham, UK, 1999, pg 767

[19] Gere, J. M., Timoshenko, S. P. Mechanics of Materials, (4th SI edition), Stanley Thornes (Publisher) Ltd, Cheltenham, UK, 1999, pg 757-758

[20] Gere, J. M., Timoshenko, S. P. Mechanics of Materials, (4th SI edition), Stanley Thornes (Publisher) Ltd, Cheltenham, UK, 1999, pg 759

[21] Gere, J. M., Timoshenko, S. P. Mechanics of Materials, (4th SI edition), Stanley Thornes (Publisher) Ltd, Cheltenham, UK, 1999, pg 773

[22] Shigley, J.E., Mischke, C. R.. Mechanical Engineering Design (5th edition), McGraw-Hill, 1989, pg 123-125

[23] Gilman, J.W., et al. Flammability studies of polymer layered silicate (clay) nanocomposites. National Institute of Standards and Technology Annual Conference on Fire Research Book of Abstracts NISTIR 6242(November) 1998. pg 37.

[24] McFarland, Andrew W. Production and Analysis of Injection Molded Micro-optics components, Master of Science Thesis, Summer, 2002, Georgia Institute of Technology, pg 66

[25] Datasheet of RenShape SL5510 photo sensitive polymer, Vantico http://www.renshape.com/ourProducts/stereolithography/pdfs/tds/northAmerica/usEnglish/SL5510_viper.pdf

[26] Datasheet of WaterClear 10120 photo sensitive polymer, DSM Somos http://www.dsmsomos.com/downloads/product_data_sheets/english/somos10120product_data_sheet.pdf